T.C.
SÜLEYMAN DEMİREL UNIVERSITY
GRADUATE SCHOOL OF NATURAL AND APPLIED SCIENCES

TRANSITION METAL ZINC DOPED TITANIUM DIOXIDE THIN FILM DEPOSITION AND CHARACTERIZATION

Zinah Hafedh Taha AL-SALIHI

Supervisor
Asst. Prof. Dr. Murat KALELİ

THE DEGREE OF MASTER OF SCIENCE
DEPARTMENT OF PHYSICS
ISPARTA - 2018

APPROVAL OF THE THESIS

"Transition Metal Zinc Doped Titanium Dioxide Thin Film Deposition and Characterization" submitted by **Zinah Hafedh Taha AL-SALIHI** in partial fulfillment of the requirements for the degree of **Master of Science** in **Department of Physics**, Graduate School of Natural and Applied Sciences, Süleyman Demirel University by,

Supervisor	**Asst. Prof. Dr. Murat KALELİ** Süleyman Demirel University	
Committee Member	**Prof. Dr. Nuri ÖZEK** Süleyman Demirel University	
Committee Member	**Prof. Dr. Rıdvan ÜNAL** Uşak University	

Director **Assoc. Prof. Dr. Şule Sultan UĞUR**

COMMITMENT

I hereby declare that all information in this document has been obtained and presented in accordance with academic rules and ethical conduct. I also declare that, as required by these rules and conduct, I have fully cited and referenced all material and results that are not original to this work.

Zinah Hafedh Taha AL-SALIHI

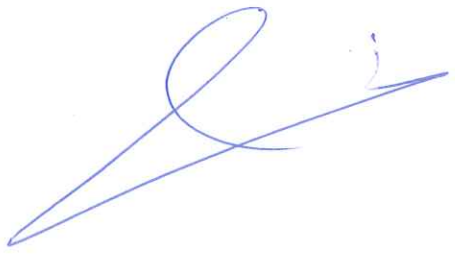

TABLE OF CONTENTS

Page

TABLE OF CONTENTS i
ABSTRACT iii
ÖZET iv
ACKNOWLEDGMENTS v
LIST OF FIGURES vi
LIST OF TABLES viii
LIST OF SYMBOLS AND ABBREVIATION ix
1. INTRODUCTION 1
1.1. Titanium dioxide (TiO_2) Material 1
1.2. Crystal structure of TiO_2 1
1.2.1. Anatase Phase of TiO_2 2
1.2.2. Rutile Phase of TiO_2 3
1.2.3. Brookite Phase of TiO_2 4
1.3. Chemical and Physical Properties of TiO_2 5
1.4. Application of titanium dioxide (TiO_2) 5
1.4.1. Photocatalytic water-splitting 5
1.4.2. Dissolution of pollutants by photocatalytic reaction 7
1.4.3. Solar cell applications of TiO_2 7
1.4.3.1. Dye-Sensitive Solar Cell (DSSC) 8
1.4.3.2. Perovskite Solar Cell 10
2. DOPING MATERIALS FOR TiO_2 12
2.1. Introduction 12
2.2. Mechanism of Doping 13
2.3. Doped Titanium dioxide TiO_2 14
2.3.1. Titanium dioxide TiO_2 doping with transition metals 14
2.3.2. Titanium dioxide TiO_2 doping with nonmetals 15
2.3.3. Zinc-doped titanium dioxide TiO_2 16
3. THIN FILM DEPOSITION TECHNIQUES 18
3.1. Introduction 18
3.2. Physical Deposition Technique 19
3.2.1. Physical vapor deposition (PVD) 19
3.2.1.1. Sputtering 20
3.2.1.2. Pulse Laser Deposition (PLD) 20
3.2.1.3. Molecular Beam Epitaxy (MBE) 21
3.2.2. Chemical vapor deposition (CVD) 21
3.2.2.1. Doctor Blade Technique 21
3.2.2.2. Spin-Coating 22
3.2.2.3. Dip-coating 23
3.2.2.4. Ultrasonic Spray Pyrolysis (USP) Technique 23
3.2.2.5. Types of Spray Pyrolysis Systems 25
3.2.2.6. The affecting factors for USP 26
4.1. Introduction 30
4.2. Thin Film Production 30

4.2.1. Substrate cleaning 30
4.2.2. Precursor Solution Composition 31
4.2.3. Ultrasonic Spray Pyrolysis preparation 31
4.2.4. Annealing 32
4.3. Thin film characterization 32
4.3.1. Scanning electron microscope (SEM) 32
4.3.2. Atomic Force Microscope (AFM) 33
4.3.3. X-Ray Diffraction (XRD) 34
4.3.4. Bragg's law 34
4.3.5. X-ray diffraction pattern 35
4.3.6. UV-vis spectrophotometer 35
4.4. Device Production 36
5. RESULT AND DISCUSSION 38
5.1. Structure Properties XRD Measurement 38
5.2. Surface Morphology of the Films (SEM) 42
5.3. Surface Topography Measurements (AFM) 48
5.4. Optical Properties UV Measurement: Optical Properties 51
5.5. The Electrical Characterization of Dye-Sensitized Solar Cell 54
6. CONCLUSION 57
REFERENCE 60
CURRICULUM VITAE 65
ÖZGEÇMİŞ 66

ABSTRACT

Master of Science

TRANSITION METAL ZINC DOPED TITANIUM DIOXIDE THIN FILM DEPOSITION AND CHARACTERIZATION

Zinah Hafedh Taha AL-SALIHI

Süleyman Demirel University
Graduate School of Natural and Applied Sciences
Department of Physics

Supervisor: Asst. Prof. Dr. Murat KALELİ

In this study, Zinc (Zn) doped Titanium dioxide (TiO_2) was deposited on glass substrates by Ultrasonic Spray Pyrolysis (USP) technique at 300 ˚C substrate temperature with 8, 16, and 25 ml solution volumes. Metal doping used to increase the structural and electrical properties of the films. Thin films surface morphology investigated by scanning electron microscopy (SEM) and it showed that there are spherically shaped microcrystals of TiO_2 and the film becomes more uniform with dense morphology when the solution volume increase. Energy Dispersive Spectroscopy EDS which coupled with SEM was used to elemental analysis for a different area and the result was so appropriate with theoretical calculation moreover, there is no change in elements weight, the atomic percentage for all samples before and after annealing. The structural properties of the films were studied by X-ray diffraction (XRD) and the results showed that the Anatase TiO_2 peak appears after annealing the samples up to 400 ˚C. The surface topography of the films was analyzed by atomic force microscopy (AFM). AFM images of Zn-doped TiO_2 showed that the films are porous in small pinholes. The roughness increased with increasing the solution volume and decreased in the same style by increasing the annealing temperature. The band gap value range of the films was investigated by UV-Vis spectroscopy and calculations showed that E_g = 3.82, 3.78, and 3.78 eV for as-grown and E_g = 3.84, 3.78, and 3.72 eV for annealed samples, from Tauc plot E_g=3.493, 3.473 and 3.498 eV for 8 ml, 16 ml and 25 ml annealed samples respectively. For solar cell device application; the solution of Zn doped TiO_2 deposited on ITO glass substrate, then these thin films were soaked in Ru dye for two days. Another two ITO glass covered with graphite to use as an anode electrode. The iodide electrolyte has been injected between the anode and cathode. The electrical properties were studied by a Current-Voltage measurement system, the results showed that the efficiency of the films was decreased after Zinc doping from 1.12 to 1.04 %, diminution of electrical fill factor FF, and increasing in current density J.

Keywords: TiO_2, Ultrasonic Spray Pyrolysis, Zn Doping, Thermal Annealing, Dye-Sensitive Solar Cell.

2018, 67 pages

ÖZET

Yüksek Lisans

ÇİNKO GEÇİS METALİ KATKILI TİTANYUM DİOKSİT İNCE FİLMLERİN BİRİKTİRİLMESİ VE KARAKTERİZASYONU

Zinah Hafedh Taha AL-SALIHI

Süleyman Demirel Üniversitesi
Fen Bilimleri Enstitüsü
Fizik Anabilim Dalı

Danışman: Dr. Öğr. Üyesi Murat KALELİ

Bu çalışmada Çinko (Zn) katkılı Titanyum dioksit (TiO_2), cam yüzeyler üzerine Ultrasonik Püskürtme Pirolizi (USP) tekniği ile 300 ˚C substrat sıcaklığında 8, 16 ve 25 ml çözelti hacimlerinde biriktirilmiştir. Filmlerin yapısal ve elektriksel özelliklerini arttırmak için metal katkılama kullanılmıştır. Taramalı elektron mikroskobu (SEM) ile incelenmiş ince film yüzey morfolojileri; TiO2'nin küresel mikro kristaller şeklinde olduğunu ve çözelti hacmi arttığında filmin yoğun morfolojiyle daha homojen hale geldiğini göstermiştir. SEM ile birleştirilen Enerji Dağılım Spektroskopi (EDS), farklı alanlarda element analizi için kullanılmış ve sonuç teorik hesaplamayla uygun bulunmuştur ki, elementlerin ağırlığında, tavlama öncesi ve sonrası tüm örneklerin atomik yüzdesinde herhangi bir değişiklik yoktur. Filmlerin yapısal özellikleri X-ışını difraksiyonu (XRD) ile incelenmiş ve sonuçlar 400 ˚C'de örneklerin tavlanması sonrasında anataz TiO_2 pikinin ortaya çıktığını göstermiştir. Filmlerin yüzey topografisi atomik kuvvet mikroskobu (AFM) ile analiz edilmiştir. Zn-katkılı TiO2'nin AFM görüntüleri, filmlerin küçük iğne delikleri şeklinde gözenekli olduğunu göstermiştir. Pürüzlülük, çözelti hacminin artmasıyla artmış ve tavlama sıcaklığını artmasıyla aynı tarzda azalmıştır. Filmlerin yasak bant aralığı değerleri UV-Vis spektroskopisi ile incelenmiş ve hesaplamalar, büyütülmüş halleriyle Eg = 3.82 - 3.78 eV ve tavlanmış halleriyle Eg = 3.84 – 3.72 eV olduğunu göstermiştir. Güneş pili cihaz uygulaması için; Zn katkılı TiO_2 çözeltisi ITO cam altlık üzerine biriktirilmiş ve daha sonra bu ince filmler iki gün boyunca Ru boyasına batırılmıştır. Anot elektrodu olarak kullanılacak başka iki ITO camı, grafit ile kaplanmıştır. İyodür elektroliti anot ve katot arasında enjekte edilmiştir. Elektriksel özellikler bir Akım-Gerilim ölçüm sistemi ile incelenmiş ve sonuçlar Çinko katkısının, elektriksel dolgu faktörünün FF'sinin azalması ve akım yoğunluğunda J'nin artmasından sonra filmlerin veriminin % 1.12'den % 1.04'e düştüğünü göstermiştir.

Anahtar Kelimeler: TiO_2, Ultrasonik Sprey Piroliz, Zn Katkılama, Tavlama, Boya Duyarlı Güneş Gözesi.

2018, 67 sayfa

ACKNOWLEDGMENTS

I want to put this page lively moments of the conclusion of this study, and I am proud of them and seize the opportunity to thank those people who were necessary to do this work.

I would like to express my deep gratitude to my supervisor, Asst. Prof. Dr. Murat KALELİ for his guidance and encouragement throughout the process of writing the thesis. His invaluable comments on the chapters of the thesis enrich the whole work and for his words that always encourage me to work hard. I feel indebted to our teamwork in Hydrogen Technology Research and Application Center (HITEM), Murat Koç, Salih Akyürekli, Esin EREN, C. Alp Yavru, and Ahmet Bayram, for them helpful and brotherly treatment. This thesis is a successful result of the joint work with my supervisor Asst. Prof. Dr. Murat KALELİ, all my sincere gratitude and appreciation to his again. I would like to express my profound gratitude to the head of the department of physics and all the professors of the department.

I am greatly indebted to my family, I would like to thanks to my husband and my children, Thanks to all my friends who have supported me and advised me.

Zinah Hafedh Taha AL-SALIHI
ISPARTA, 2018

LIST OF FIGURES

Page

Figure 1.1. TiO_2 nanopowder 1
Figure 1.2. Anatase TiO_2 tetragonal structure (Ti grey, O red) 3
Figure 1.3. Rutile TiO_2 tetragonal structure (Ti grey, O red) 3
Figure 1.4. Brookite TiO_2 orthorhombic structure (Ti grey, O red) 4
Figure 1.5. Mechanisms of TiO_2 photocatalytic for splitting water 6
Figure 1.6. TiO_2 particle photocatalytic in pollutant water 7
Figure 1.7. Best Research-Cell Efficiencies until 2020 8
Figure 1.8. The DSSC structure and layers 8
Figure 1.9. The DSSC working principle 9
Figure 1.10.The crystal structure of perovskite ABX3 10
Figure 1.11. Perovskite solar cell layers; electron-hole transferring and band diagram 11
Figure 2.1. Scheme for a possibility of dopants in lattice 12
Figure 2.2. Doping mechanisms of polycrystalline TiO_2 14
Figure 2.3. The band gap for undoped, substitutional N doped and interstitial N doped TiO_2 15
Figure 3.1. Scheme of chemical deposition techniques 18
Figure 3.2. Scheme of physical deposition techniques 19
Figure 3.3. Physical vapor deposition technique 19
Figure 3.4. Scheme of the morphology of PVD 20
Figure 3.5. Dr. Blade system 22
Figure 3.6. a) Spin Coating device b) Scheme showed the steps of spin coating 22
Figure 3.8. Scheme of dip coating stages 23
Figure 3.9. Ultrasonic Spray Pyrolysis system (USP) 24
Figure 3.10. Agglomerated particles inside the solution dispersed by ultrasonic vibration 24
Figure 4.1. Photo of the oven which annealing held under atmosphere 32
Figure 4.2. Scanning electron microscope system (SEM) 32
Figure 4.3. Atomic Force Microscope (AFM) 33
Figure 4.4. X-Ray diffraction (XRD) system (Bruker D8 Advance Twin-Twin). 34
Figure 4.5. X-ray diffraction 35
Figure 4.6. Electronic transition 36
Figure 4.7. Zn doped TiO_2 on ITO glass substrate annealed up to 470 ˚C 36
Figure 4.8. a) Photo of 16 ml of Ru – Zn doped TiO2 B) 8 ml of Ru - Zn doped TiO_2 on ITO glass was soaked Ru ruthenium (II) dye $C_{58}H_{96}N_8O_8RuS_2$ 37
Figure 4.9. a) Before electrolyte injection b) KI electrolyte injected and c) current-voltage measurements under light/dark 37
Figure5.1. Patterns of Zn-doped TiO2(8 at. %) for 8 ml, 16 ml, and 25 ml deposition volumes annealed up to 550 patterns of Zn doped TiO_2 (8 at. %) for 8 ml, 16 ml, 25 ml deposition volumes annealed up to 550 ˚C 39
Figure 5.2. XRD pattern of Zn doped TiO_2 (8 at. %) annealed at different temperatures start from (300 ˚C to 550 ˚C sequentially) 40
Figure 5.3. S-Q represent the ratio of the crystal of the TiO_2 film 41

Figure 5.4. XRD pattern of Zn dopant TiO_2 annealed up to 550 ˚C 42
Figure 5.5. SEM images of (a) 8 ml for as-grown sample (b) 8 ml annealing (550 ˚C) (c) 16 ml for as-grown (d) 16 ml annealing sample (e) 25 ml for as-grown (f) 25 ml annealing sample 43
Figure 5.6. The thickness of 25 ml ~ 420 nm thin films after annealing up to 550 ˚C 44
Figure 5.7. SEM images for 16 ml (a) TiO_2 microparticles spherical shape with some concavity (b) size of concavity about 2.4 µm after annealing 44
Figure 5.8. EDS result for element analysis 8 ml as-grown sample 45
Figure 5.9. EDS result for element analysis 8 ml annealed sample 45
Figure 5.10. EDS result for element analysis 16 ml as-grown sample 46
Figure 5.11. EDS result for element analysis 16 ml annealed sample 46
Figure 5.12. EDS result for element analysis 25 ml as gown sample 47
Figure 5.13. EDS result for element analysis 25 ml annealed sample 47
Figure 5.14. Image of Zn-doped TiO_2 8 ml (a) 3D and 2D image as grown with roughness R_a = 4.10 nm (b) 3D and 2D image annealing with roughness R_a = 1.16 nm 49
Figure 5.15. Image of Zn-doped TiO_2 16 ml (a) 3D and 2D image as grow with roughness R_a = 7.47 nm (b) 3D and 2D image annealing with roughness R_a = 1.40 nm 50
Figure 5.16. Image of Zn-doped TiO_2 25 ml (a) 3D and 2D image as grown with roughness R_a = 15.13 nm (b) 3D and 2D image annealing with roughness R_a = 3.51 nm 50
Figure 5.17. The relation between wavelength and absorption of a Zn-TiO_2 thin film for different fluid volume 52
Figure 5.18. a, b, and c the relation between wavelength and absorption of a Zn-TiO_2 thin film for 8 ml,16 ml, 25 ml respectively 52
Figure 5.19. The bandgap value from Tauc equation for a) 8 ml, b) 16 ml, c) 25 ml annealed samples 54
Figure 5.20. Current-Voltage curve for DSSC of bare TiO_2 dark - light 56
Figure 5.21. Current-Voltage curve for DSSC of Zn doped TiO_2 dark - light 56

LIST OF TABLES

Page

Table 1.1. TiO_2 crystal system for natural and synthesis form 2
Table 1.2. Structure properties with unite cell of Rutile, Anatase, Brookite-TiO_2 4
Table 1.3. Physical and chemical properties of TiO_2 5
Table 3.1. Comparison between CD and PD deposition technique 21
Table 3.2. Droplet size and atomization rate according to atomizer 25
Table 5.1. The relation between annealing temperatures for (25 ml sample) and crystal size D 40
Table 5.2. The crystal size for different fluid volume (annealed up to 550 ℃) 39
Table 5.3. Crystal lattice parameters 40
Table 5.4. Involving the composition of elements, weight and the atomic percentage of 8 ml as-grown sample 45
Table 5.5. Explain the composition of elements, weight and the atomic percentage of 8 ml annealed sample 46
Table 5.6. Involving the composition of elements, weight and the atomic percentage of 16 ml as-grown sample 46
Table 5.7. Involving the composition of elements, weight and the atomic percentage of 16 ml annealed sample 47
Table 5.8. Involving the composition of elements, weight and the atomic percentage of 25ml as-grown sample 47
Table 5.9. Involving the composition of elements, weight and the atomic percentage of 25 ml annealed sample 48
Table 5.10. The changing of roughness with fluid volume before and after annealing 49
Table 5.11. The relation between wavelength λ and bandgap for as-grown samples. 53
Table 5.12. The relation between wavelength λ and bandgap for annealed samples 53
Table 5.13. Comparison between bare TiO_2 and doped TiO_2 for DSSC parameters 55

LIST OF SYMBOLS AND ABBREVIATION

$\bar{\nu}$	Wavenumber
$^{\circ}C$	Degree Celsius
A	Absorption
at. %	Atom percentage
B	FWHM (Full Width Half Maximum)
C	The light speed in the vacuum
d	Atomic layer spacing/distance
D	Crystal size
DSSC	Dye-Sensitive Solar Cell
eV	Electron-volt
FF	Electrical fill factor
GPa	Giga Pascal
$h\nu$	Photon energy
I_{mp}	Current at a maximum point
I_{mp}	Short circuit current
N	Multiple integers of the X-ray wavelength λ
P	Pressure
R_a	Roughness average
Ru	Ruthenium (II) dye
T	Absolute temperature
t	Thickness of thin film
V_{mp}	Voltage at a maximum point
V_{oc}	Open circuit voltage
η	Efficiency of DSSC
θ	Angle of the interference
λ	Wavelength
psi	Pound per square inch.
ν	The light speed in a matter

1. INTRODUCTION

1.1. Titanium dioxide (TiO_2) Material

Titanium dioxide is one of the important metal oxide n-type semiconductors with a wide band gap value (~3.2 eV). It has a wide application area in nanotechnology field because of it's beneficial optical and physical properties such as non-toxic, low cost, chemically stable, high refractive index and high photocatalytic activity (Z.Yahya, 2010).

Figure 1.1. TiO_2 nanopowder (Chamandy, 2014)

Titanium dioxide is known as titania and used as a white pigment because of brightness and high refractive index n ≈ 2.7 (Chowdary et al., 2012). Titanium dioxide is used as a powder form if it used as a pigment to provide whiteness and opacity to products such as paints, coating, plastics, papers, inks, food, medicines, as well as most toothpaste. The opacity improved by arranging the ideal size of TiO_2 particles.

1.2. Crystal structure of TiO_2

The main three crystal phases of TiO_2 are Anatase (tetragonal), Rutile (tetragonal), and Brookite (orthorhombic). It has a band gap around ~3.2 eV (Essalhi et al., 2016). The most common and chemically stable phases are Rutile and Anatase. It can be excited by light which has a wavelength less than 390 nm. Anatase phase transfer to Rutile in elevates temperatures. Brookite cannot be excited by UV light and not a stable phase but it can be transferred to the Rutile phase by thermal annealing. In addition to main Rutile, Anatase, and Brookite phases; there are eight modification

phases; three of them stable and other five can be produced just synthetically which are shown in Table 1.1. (Li and Liu 2016). The last five phases refer into plenty high-pressure structures of TiO_2.

Table 1.1. TiO_2 crystal system for natural and synthesis form (Li and Liu 2016)

Form	Crystal system	Synthesis Conditions
Anatase	Tetragonal	
Rutile	Tetragonal	
Brookite	Orthorhombic	
TiO_2 (B)	Monoclinic	Hydrolysis of $K_2Ti_4O_9$ followed by heating
TiO_2 (R)	Orthorhombic	oxidation of related lithium titanate bronze $Li_{0.16\ ml}TiO_2$
TiO_2 (H)	Tetragonal	oxidation of related potassium titanate bronze $K_{0.16\ ml}TiO_2$
TiO_2 (ll) (α-PbO_2-like form)	Orthorhombic	
Baddeleyite (seven coordinate Ti)	Monoclinic	
Cubic form	Cubic	P > 40 GPa T > 1600 ˚C
TiO_2(Oll) cotunnite;($PbCl_2$)-	Orthorhombic	P > 40 GPa T > 700 ˚C
TiO_2(OI)	Orthorhombic	

1.2.1. Anatase Phase of TiO_2

It is one of the non-stable phase addition to the Brookite phase. In annealing processes above 700 ˚C, all Anatase phase converts to Rutile phase. In some other work, it is found that 500 ˚C thermal treatment is enough for phase transition from Anatase to Rutile. Anatase structure is tetragonal and can be seen in Figure 1.2. Lattice parameter a = b = 3.784 Å, c = 9.515 Å and a/c ratio of 0.3976 (Zallen and Moret 2006). In low temperatures (below 273 ˚C), Anatase is more stable than Rutile but the energy differences between these two phases smaller than (2 to 10 kJ/mol) (Muscat, Swamy, and Harrison, 2002). In solar cell application, the TiO_2 Anatase phase is preferred than other polymorphs phases because of high mobility, low dielectric constant, and low density. The high Fermi level of Anatase phase increase the photoreactivity and also lowers the adsorption of oxygen (higher hydroxylation) (Tanaka, Capule, and Hisanaga, 1991).

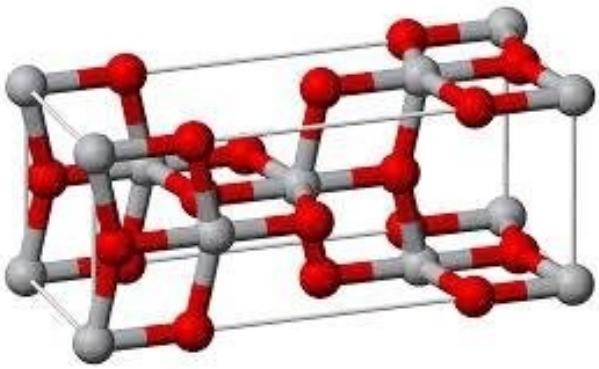

Figure 1.2. Anatase TiO_2 tetragonal structure (Ti grey, O red) (Fatima Javed et al., 2015)

1.2.2. Rutile Phase of TiO_2

Rutile phase is the more stable phase at high temperatures and pressures up to 6 Kbar. It contains 6 atoms per unit cell which shown in Figure 1.3. and the lattice parameters are a = b = 4.5936 Å, c = 2.9587 Å with c/a ratio of 0.64409 (Zallen and Moret, 2006).

The transformation of phase structure by thermal annealing causes change in particle size until reaching to a certain size (for particles bigger than 14 nm) and Rutile become more stable than the other phases. As photocatalysts, the activity of Rutile is very low comparing with Anatase, hence Rutile can be considered active or non-active depending on preparation conditions (Kessler, 2014).

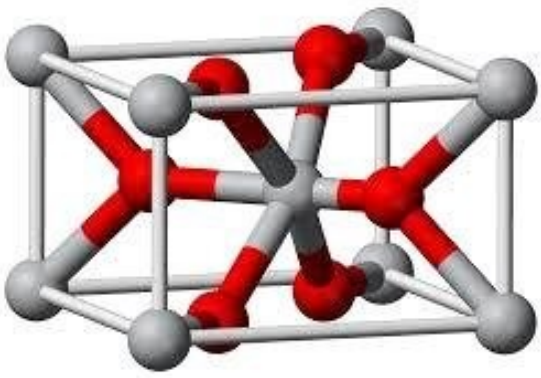

Figure 1.3. Rutile TiO_2 tetragonal structure (Ti grey, O red) (Fatima Javed et al., 2015)

1.2.3. Brookite Phase of TiO_2

The Brookite is a more complicated phase and has a bigger cell volume than Rutile and Anatase phases. It is not used in experimental research because it is just a transitional phase (Z.Yahya, 2010). Brookite phase unit cell is shown in Figure 1.4.

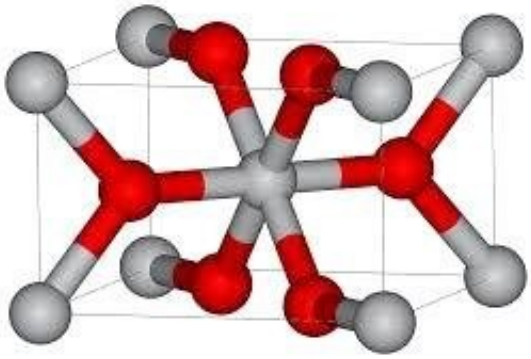

Figure 1.4. Brookite TiO_2 orthorhombic structure (Ti grey, O red) (Fatima Javed et al., 2015)

The Ti-O bond lengths, Ti-O-Ti bond angle in Brookite is bigger than Anatase and Rutile phase as given in Table 1.2.

Table 1.2. Structure properties with unite cell of Rutile, Anatase, Brookite-TiO_2 (Kessler, 2014)

Properties	**Rutile**	**Anatase**	**Brookite**
Crystal structure	Tetragonal	Tetragonal	Orthorhombic
Lattice constant (Å)	a=4.5936 c=2.9587	a=3.784 c=9.515	a=9.184 b=5.447 c=5.154
Space group	$P4_2/mnm$	$I4_1/amd$	Pbca
Molecule (cell)	2	2	4
Volume/molecule ($Å^3$)	31.2160	34.061	32.172
Density ($g.cm^{-3}$)	4.13	3.79	3.99
Bond length (Å)Ti-O	1.949(4) 1.980(2)	1.937(4) 1.965(2)	1.87-2.04
Bond angle O-Ti-O	81.2° 90.0°	77.7° 92.6°	77.0°-105°

Various production parameters can create these phases such as pressures, temperature, and the source of material (rock formations in the earth). Because of the difference between these crystal systems, the optical properties of each phase are slightly different such as absorption band gap value was found as 3.00, 3.20 and 3.50

eV for Rutile, Anatase, and Brookite respectively (Ruzybayev et al. 2015; Zallen and Moret 2006) Also, Anatase phase Fermi level has slightly higher (0.1 eV) than the other phases. For thin film application, Anatase phase has higher mobility than other phases and it is more efficient in terms of photocatalytic activity (Zallen and Moret 2006).

1.3. Chemical and Physical Properties of TiO_2

In recent years, many processes and technique are developed to synthesize TiO_2 Nanopowder and thin films with a different crystalline structure. The properties of TiO_2 depend on synthesizing method and conditions. Some of the chemical and physical properties of the TiO_2 are summarized in Table 1.3.

Table 1.3. Physical and chemical properties of TiO_2 (Z.Yahya, 2010)

Molecular formula	TiO_2
Color and form	White powder
Crystallite size	Amorphous
Group	Ti: 4 O: 16
Electronic configuration	Ti [Ar] $3d^2 4s^2$, O [He] $2s^2 2p^4$
Density	4.23 g/cm^3
Molecular weight	79.93 g/mol
Melting point	1.843 ˚C
Boiling point	2.972 ˚C
Chemical composition	Ti: 59.93 %, O: 40.55 %

1.4. Application of titanium dioxide (TiO_2)

Titanium dioxide has a wide range of applications in nanotechnology filed due to its physical, optical, electrical, and chemical properties. In the following chapters some of these applications will be explained:

1.4.1. Photocatalytic water-splitting

In the recent years the research trend to a new resource of energy which is not depleted when used; one of most important is “renewable energy” sources that due to

its; low cost, available locally, and uncontaminated such as wind power, potential energy of waterfalls and sea, and the greatest one solar energy (Xie et al., 2017). Hydrogen an exemplary fuel can be produced from that sources, photocatalytic water splitting one of many ways to produce hydrogen (Xie et al., 2017). High photocatalytic of nano-sized TiO_2 for splitting water has big attention due to its properties. The first study that published about water splitting was in 1972 by Honda and Fujishima. They used the Rutile form of the TiO_2 as anode and platinum as a cathode to split water into oxygen and hydrogen (Yuri F. Zhukovskii, Sergey Piskunov, Oleg Lisovski, 2016). The mechanisms of TiO_2 photocatalytic for water splitting shown in Figure1.5.

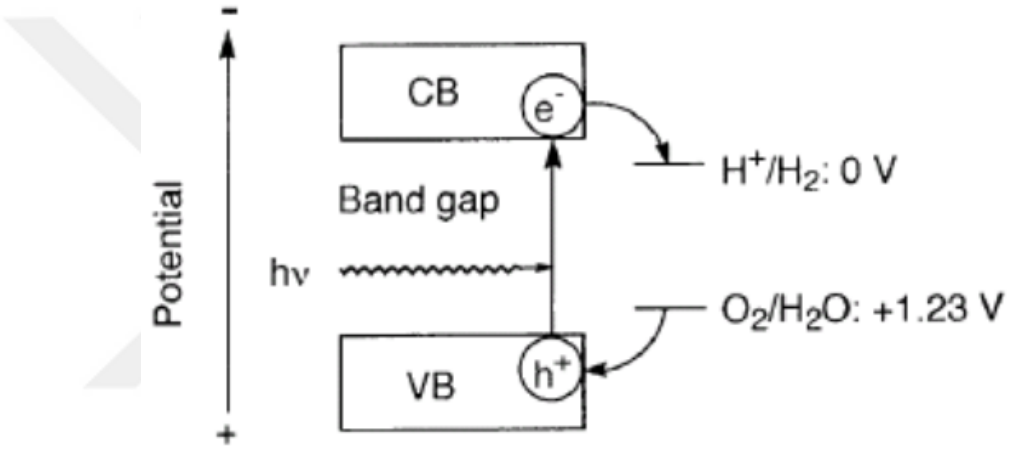

Figure 1.5. Mechanisms of TiO_2 photocatalytic for water splitting (Chi-Hung Liao et al., 2012)

The band gap value of semiconductor plays an important role in photocatalytic activity, when a photon has energy equal to the band gap, the electrons ($\bar{e}$) will be excited from valance band VB to the conduction band CB after gain over extra energy and leaving an empty space (h^+) as explain in the following equation:

$$TiO_2 + hv \rightarrow \bar{e} + h^+ \qquad 1.1$$

The recombination of electron-hole will happen in brief time and lose the energy as a heat or photon, only the electrons, and holes which have higher energy can be bail up to the surface of semiconductor to involved in reduction and oxidation reaction that

lead to Photocatalytic hydrogen production and air purification also (Ni et al. 2007; Z.Yahya 2010).

1.4.2. Dissolution of pollutants by photocatalytic reaction

Titanium dioxide has a wide application as water sterilization and air purification. The photon that has energy higher than band gap value (~3.2 eV) for TiO_2 and wavelength less than $\lambda = 390$ nm will excite the electron ($\bar{e}$) from valance band VB to the conduction band and that will be generate an electron-hole pair. The electron ($\bar{e}$) in conduction band CB and the hole in valance band (h^+) will be the agents of oxidation and reduction. CO_2 and H_2O are the results after hole in the conduction band (CB) interact with organic compounds by the way of oxidation which is shown in Figure1.6 (M. Umar and H. Abdul Aziz, 2013).

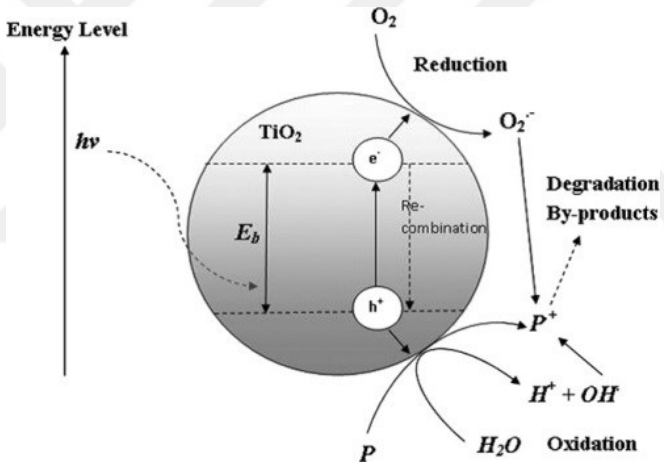

Figure 1.6. TiO_2 particle photocatalytic in pollutant water (Muhammad Umar et al., 2013

1.4.3. Solar cell applications of TiO_2

The optical and electrical properties of TiO_2 makes it feasible for a wide application in solar cell applications and optoelectronic devices (organic-inorganic and hybrid solar cell, gas sensors, etc.). Figure 1.7. shows the best efficiency in solar cell research.

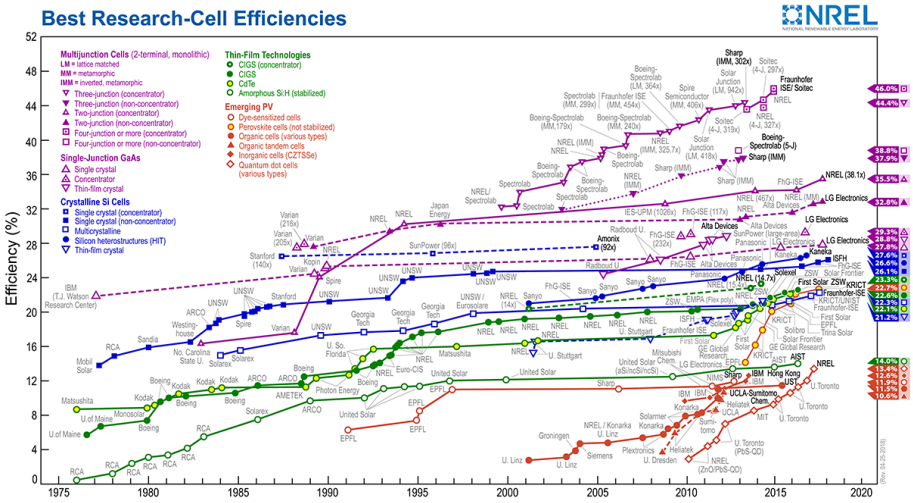

Figure 1.7. Best Research-Cell Efficiencies until 2020 (NREL best efficiency chart 2018)

1.4.3.1. Dye-Sensitive Solar Cell (DSSC)

In 1988 Michael Grätzel and Brian O'Regan invent the DSSC solar cell which is belonging to the third generation of thin film solar cell, so it's called "Grätzel cell". The first publication for higher efficiency was in 1991 (Chu, 2011). The solar cell can be made from cheap materials which are shown in Figure 1.8.

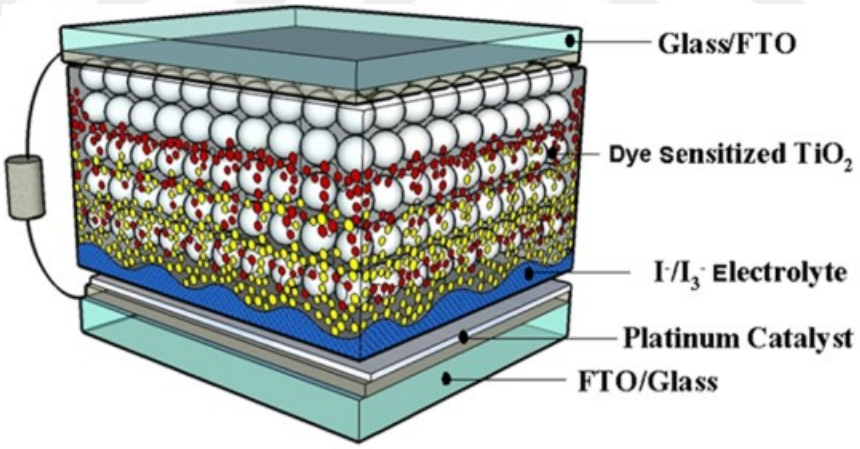

Figure 1.8. The DSSC structure and layers (Schanze Research Group, 2014)

These solar cells consist of:

- A transparent conducting oxide-coated substrate (TCO) such as ITO Indium-tin oxide which has low resistance at room temperature (or FTO fluorine-tin oxide).
- Semiconductor materials as a photoelectrode like (Si, GaAs, InP, CdS, etc.) but TiO_2 is the most chemical stable one.

- Ru complex like photosensitizers (dye) which are adsorbed onto TiO_2, ($C_{30}H_{24}N_6CL_2RI.6H_2O$) (a different compound with high absorption capability reaching to IR-region (400 nm-900 nm)).
- Redox electrolyte that contains $\bar{I}/\bar{I}_3$ redox ions, and a counter electrode that has high electrocatalytic
- A thin plate of platinum catalyst (Z.Yahya, 2010).

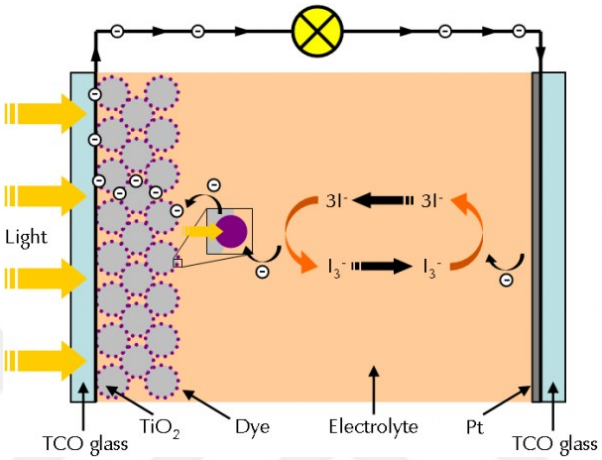

Figure 1.9. The DSSC working principle (Gamry Instrument, 2018)

The transparent layer will receive the light (photon) from sunlight or any other source, after hitting the dye on the surface of TiO_2, so the dye now on excited state which means oxidation of photosensitizer, electron will acquire an extra energy make it injected to the conduction band CB of TiO_2, and by diffusion which is happening because of gradient of electron concentration that electron transport to anode ITO or FTO. After that, the electron reaches the electrolyte $\bar{I}/\bar{I}_3$ and oxidized it to tri-iodide. This reaction obstruct the electron recombination with oxidized dye and by diffusion of the tri-iodide return the missing electron, where the counter electrode re-introduces the electrons after flowing through the external circuit (Chu, 2011).

In this process, there is no hole created only an additional electron. Although it is possible for the electron to recombine back into the dye, the rate at which this occurs is slow compared to the rate at which the dye regains an electron from the surrounding electrolyte. Recombination directly from the TiO_2 to species in the

electrolyte is also possible although, for optimized devices, this reaction is rather slow.

DSSC has many advantages; its low cost, visible light condition, a low-density application like a rooftop solar collector, ability to cell production at a lower temperature (Chu, 2011).

1.4.3.2. Perovskite Solar Cell

From the name, it's clear that the cell includes a compound which is derived from the crystal structure "perovskite" is given in Figure 1.10. This absorber materials with the same type of crystal structure as calcium titanium oxide $CaTiO_3$ (Kojima et al., 2009).

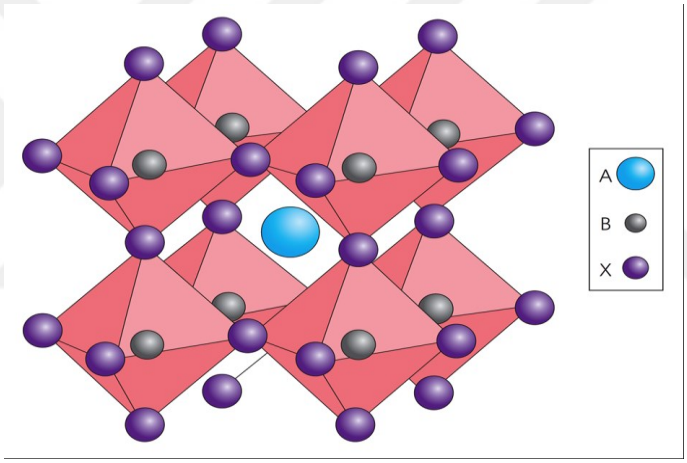

Figure 1.10. The crystal structure of perovskite ABX3 (Alechetron, 2018)

ABX3 complex is an organic cation-methylammonium $CH_3NH_3^+$ (A), inorganic cation lead Pb^{+2} (B) and anion can be iodine $\bar{I}$, bromine $\overline{Br}$, or chloride $\bar{Cl}$ (X3) (Manser, Christians, and Kamat, 2016) . In recent years, the perovskite has a great interest due to an excessive increase in efficiency (20% until 2015) just only a few years. The low fabrication cost, high optical absorption coefficient, high values of open- circuit voltage V_{oc} , the high diffusion length of electron-hole, direct band gap ~1.55 eV and high charge carrier mobility makes the perovskite solar cell popular (Manser et al., 2016). Figure 1.11. explains the consisting layers of perovskite solar cell.

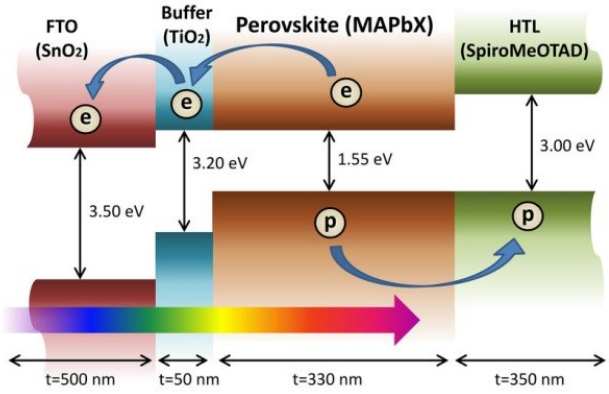

Figure 1.11. Perovskite solar cell layers; electron-hole transferring and band diagram (Olyaefer et al., 2017)

Titanium dioxide has a lot of applications that cannot mention in details in this thesis such as; pigments, UV-resistant material for cosmetic (because of high refractive index its use in sunscreen), whitening cream, paper, plastic, antibacterial compositions (due to good photocatalytic properties), self-cleaning surfaces (Pilkington" active glass), also TiO_2 use in antireflection coating, sterilize water, air purifier.

2. DOPING MATERIALS FOR TiO_2

2.1. Introduction

Controlled impurity or doping is one of the most functional methods in modifying the properties of semiconductor materials. Adding the dopant material in an identical way, there will be two possibilities either an unsettled oxide phase or a second phase which depending on solubility limit of two combination dopant and precursor solution. Physical parameters of the constituent materials; ionic size and electronegativity or diffusion process effects on the doping mechanism. As is evident by doping the electronic structure, surface structure, and phase structure can be changed. Semiconductors are doped by defects or impurity; these impurities can act as donor or acceptor. When the defects release the electron to the conduction band (CB) they are called “donors” while impurities that remove holes to the valence band (VB) they are called “acceptors”. Dopants materials can stay either as a substitutional or interstitial position in the crystal structure. Commonly, the defects can be found as vacancies, interstitials, dislocations and antisites forms which can be seen in Figure 2.1. (Cotutelle et al., 2013).

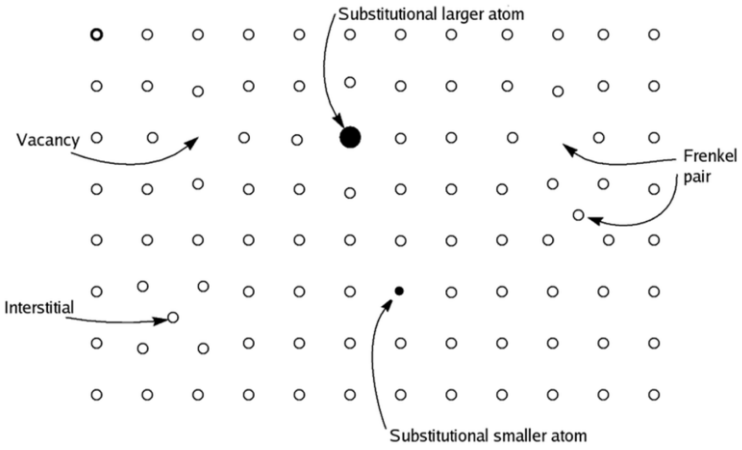

Figure 2.1. Scheme for a possibility of dopants in a crystal lattice (Rajesh Pandiyan, 2013)

2.2. Mechanism of Doping

There is a different type of doping mechanism which makes the distributions of dopants various and different effects on semiconductor electro-optical properties; such as:

- The doping that effects on properties by describing surface coverage with small islets which are depending on the size of the particles, the covering of surface, and the interface created between particles as shown in Figure 2.2a.
- In Figure 2.2b indicate to the doping by forming a thin oxide layer by extends the dopant over the surface and straight the boundaries of grain, this type of doping can be produced a clogging on the surface of host lattice (polycrystalline TiO_2).
- Permeation the boundary grain by dopant in elevated temperatures (In Figure 2.2c).
- Penetration the dopants into the grains (Cotutelle et al., 2013) as shown in Figure.2.2d, the change of semiconductor properties are not clear (not well-defined) because of the gradients of dopant concentration. But if the system reaches the equilibrium (gas/solid stage) the homogeneity of dopant distributed increase and the gradients concentration of dopant disappears (In Figure 2.2e). So that type of doping can be defined as defect chemistry (Nowotny et al., 2008).

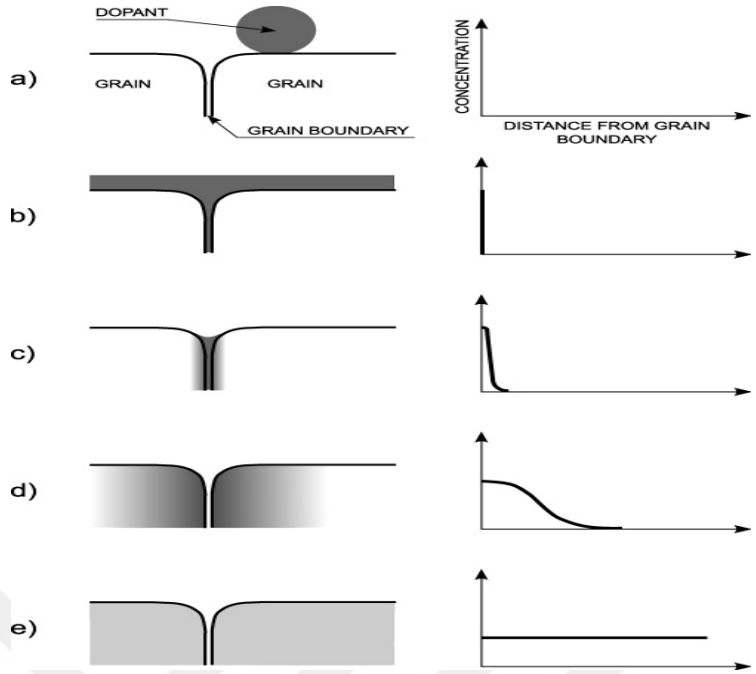

Figure 2.2. Doping mechanisms of polycrystalline TiO_2 (a) deposition of isolated islets on the surface, (b) spread of the dopants on the surface and within grain boundaries, (c) filling of grain boundaries leading to limited diffusion profile, (d) limited bulk transport leading to the formation of a concentration gradient, and (e) homogeneous distribution of the dopant within the specimen (Rajesh Pandiyan, 2013)

2.3. Doped Titanium dioxide TiO_2

Many research and investigation have been studied about doping which is a way to altering the properties of a semiconductor such as narrowing band gap, shifting the absorbing area for semiconductor, modifying the chemical properties, and enhancing the photocatalytic activity (Zaleska-medynska and Zaleska, 2018). Impurity (or dopant) energy levels will form within the bandgap of a semiconductor by doping and that makes electron need lower photon energy to transport to the conduction band CB.

2.3.1. Titanium dioxide TiO_2 doping with transition metals

Different transition metals are doped with TiO_2 such as Fe, V, and Mo to study doping effect by electron paramagnetic resonance. Also, TiO_2 doped with 21 different metal ions for ex. Fe(III), Mo(V), Ru(III), Os(III), Re(V) to increase the photo-reactivity. In sum, the doping of TiO_2 with metal ions increase the photochemical reactivity and it can be besieged (surrounded) the recombination rate ratio by increase photo-reduction rate which produced photocatalyst (Kessler, 2014).

The excess concentration of dopants (transition metal ions with TiO_2) have an opposite effect on photocatalytic activity because of the formation of restrict d-states in the TiO_2 band gap, all the holes transport from the VB and the electrons in the CB band will capture by restricting d-states (Kessler, 2014). And this mechanism will lead to increased band gap values.

2.3.2. Titanium dioxide TiO_2 doping with nonmetals

In 1986, TiO_2 doped with nonmetal firstly by Unruersrty et al. and they get powders form of nitrogen-doped-TiO_2 by calcification for titanium hydroxide, which is exhibit high photocatalytic activity in the visible region ~ 434 nm (Unruersrty, 1986). There is no study which getting better results until 2001. Asahi et al. reported narrowing in band gap while $TiO_{2-X}N_x$ thin films were prepared by sputtering the target of TiO_2 with ambiance ratio 40% N_2/Ar and processing the Anatase powder in 67% NH_3/Ar at 600 ˚C for 3 hours (Asahi, 2001).

There are three major ideas about nonmetal doping which can be seen in Figure 2.3: I. N doped TiO_2 narrowing bandgap due to the convergence of energies level between N and TiO_2 thus the ability to absorb visible light increasing. II. The oxygen position of TiO_2 changed by nitrogen atom that's lead to formation isolated impurity energy levels above valance band VB, but the electrons excited only in impurity energy level when illumination by visible light and in both levels with UV light. III. the nitrogen doped in some of the oxygen vacancies these vacancies which form in the grain boundaries is important to stand out vis-activity and the nitrogen will be a barrier for re-oxidation (Zaleska-medynska and Zaleska, 2018).

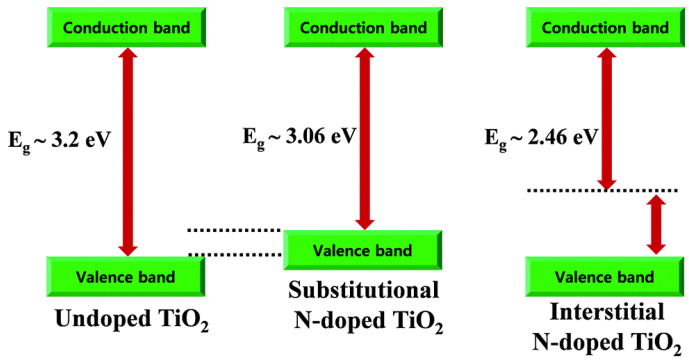

Figure 2.3. The band gap for undoped, substitutional N doped and interstitial N doped TiO_2 (Sajid Ali Ansari et al., 2016)

There is two type of N doped TiO_2 either substitutional or interstitial; in substitutional doping, a shallow acceptor state will be formed above VB while with interstitial nitrogen isolated impurity level form in the mid of band gap. There are other doping with nonmetal after succeeded of recording a high photocatalytic activity under visible light of N doped TiO_2 such as Carbon, Sulfur, Boron, Phosphorus, Flour, and Iodine (Zaleska-medynska and Zaleska, 2018)

2.3.3. Zinc-doped titanium dioxide TiO_2

Zinc (Zn) which is one of the transition metals dopants for TiO_2. In some previous studies, TiO_2 nanoparticles doped with Zn (Khairy and Zakaria, 2014). The study tried to clarify the effect of doping on the bandgap value of TiO2, by Sol-Gel method with 2 at. % dopant concentration. The result of the research referred to red-shift to lower bandgap energy (longer wavelength > 400 nm) in other words the energy that needed to activate Zn doped TiO_2 samples is lower than that required for pure TiO_2 and that means narrowing of bandgap for TiO_2 (Khairy and Zakaria, 2014). Another investigation of Zn doped TiO_2 with different concentration of dopant (2, 4, 6, and 8 at. %) by spray pyrolysis exhibits the strain of the film increased for higher concentration, the crystallinity improved for 8 at. %, moreover; for higher doping ratio (8 at. %) the grain size becomes smaller, closer, and more homogeneous (Arunachalam et al., 2015). In another work, Sol-Gel method was used to prepare a compact layer of Zn doped TiO_2 (1, 3, 5, 7 mol % of dopant) and this study showed the changes in structural properties of the TiO_2 by dopant concentrations. When doping concentration was increased, Anatase phase intensity of TiO_2 decreased, but for Rutile it increased after 3 mol % of dopant concentration. The optical properties for various doping concentration of TiO_2 with Zn such as band gap decreased with doping concentration increase (3.75, 3.73, 3.72, 3.58 and 3.26 eV for 1, 3,5, and 7 mol % respectively) and the absorption edge shifted to the red region (> 400 nm) (Wu et al., 2016) . But that study contradictory with Arunachlam et al., its exhibit the surface morphology of the film becomes unregularly and the higher concentration of doping (> 7 mol %) causes of defects structure and there is an agreement for lower concentration less than 5 mol %. There are many reasons for that defects; in higher concentration, a secondary phase of Zn_2TiO_4 will be formed on Rutile TiO_2 surface

(Wu et al., 2016). and there is another reason which was mentioned in 2.3.1; formation of restricting d-states within the TiO_2 bandgap, so this will lead to increased bandgap value (Kessler, 2014).

It's clear from the above the advantage of doping on structural and optical properties, for a doped semiconductor. But also, there are many disadvantages such as the recombination of diffusion charge carriers at dopant sites, the excess of dopant has an inverse effect on band gap value as it was discussed, and the high carrier recombination rate (metal-doped TiO_2) decreased/or no photocatalytic activity under visible light and that can be adjusted depending on the concentration of dopant and precursor solution preparation process.

3. THIN FILM DEPOSITION TECHNIQUES

3.1. Introduction

There are various deposition techniques which play an important role of thin film fabrication because of the homogeneity and physical nature of the thin film determined by deposit technique. Physical and chemical deposition techniques are the main processes of thin film deposition. Chemical deposition technique can be divided into gas and solution phase techniques which include sol-gel, dip coating, spin coating, and ultrasonic spray pyrolysis. Gas phase deposition method comprises chemical vapor deposition include Electrochemical vapor deposition (EVD) and atomic laser deposition (ALD) which can be seen in Figure 3.1 (Hamedani, 2008). Physical deposition technique includes laser ablation, molecular beam epitaxy, and physical vapor deposition which is divided in to pulse laser deposition (PLD) and sputtering which is shown in Figure 3.1 (Hamedani, 2008).

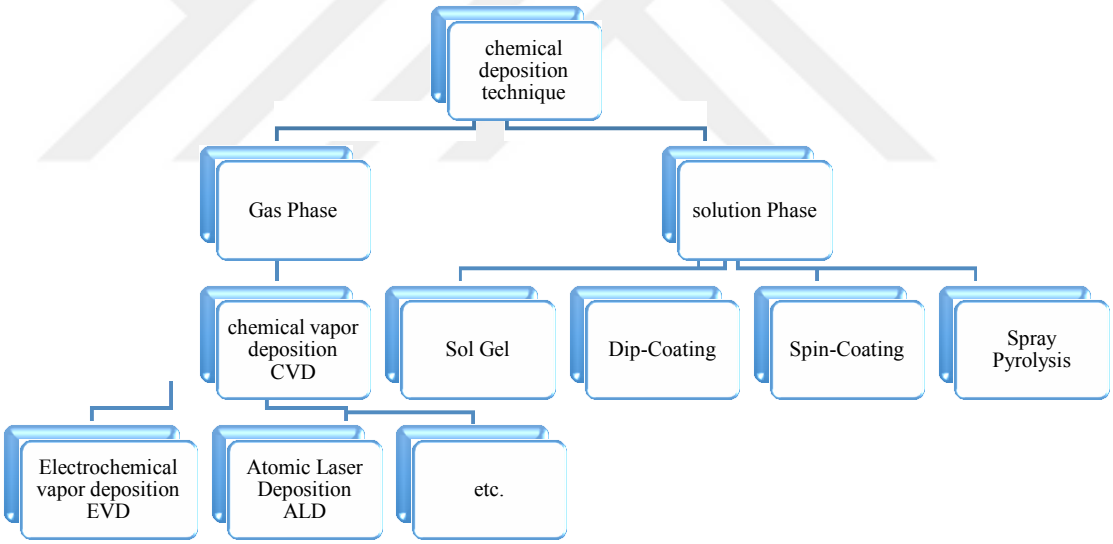

Figure 3.1. Scheme of chemical deposition techniques

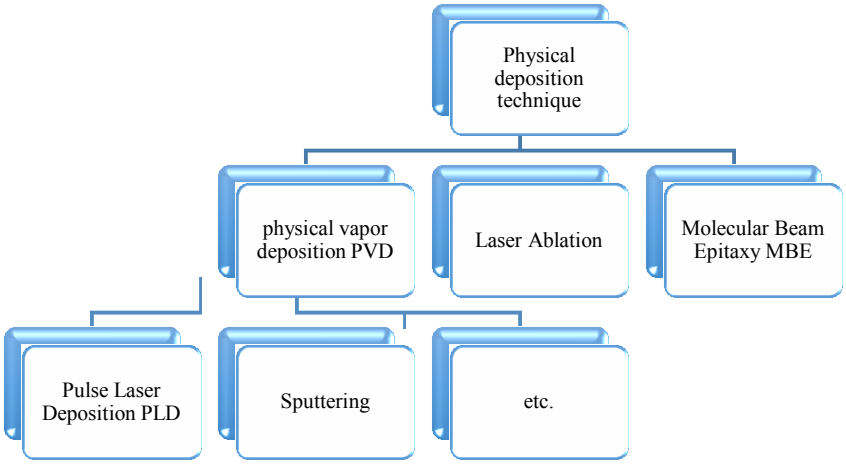

Figure 3.2. Scheme of physical deposition techniques

3.2. Physical Deposition Technique

It is one of technique that depends on evaporation either thermal or vacuum evaporation. The general steps of this technique are; source material boil over to get a vapor, the vapor transfer to a surface (substrate) and precipitate on the substrate (Seshan, 2001).

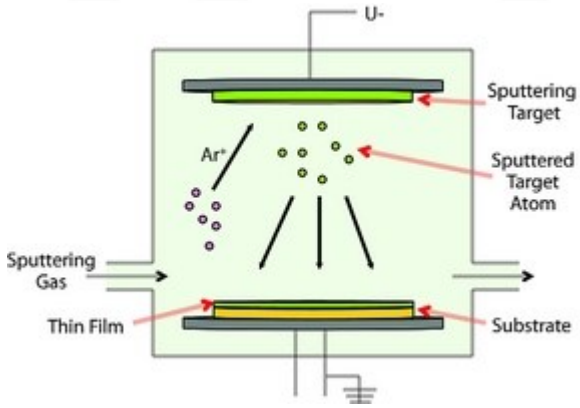

Figure 3.3. Physical vapor deposition technique (Sigma Aldrich, 2018)

3.2.1. Physical vapor deposition (PVD)

In this process, the materials vaporized from a solid or liquid source in the form of vapor through a vacuum or low pressure gaseous or plasma and evaporated on a substrate. The advantages of this process are; it can be used to deposited films within several nanometers to micrometers, the capability of forming multi-layer coatings, deposition area could be either small or large. The PVD process applied at a high

temperature (or momentum of ions) to evaporate materials (Savale, 2016). In this process, many transferring in an atomic level will take place so the target material transfer from solid or liquid to gas phase and once again to the solid phase (deposition) which is summarized in Figure 3.4. (Pahade, Chavan, and Baisane, 2016).

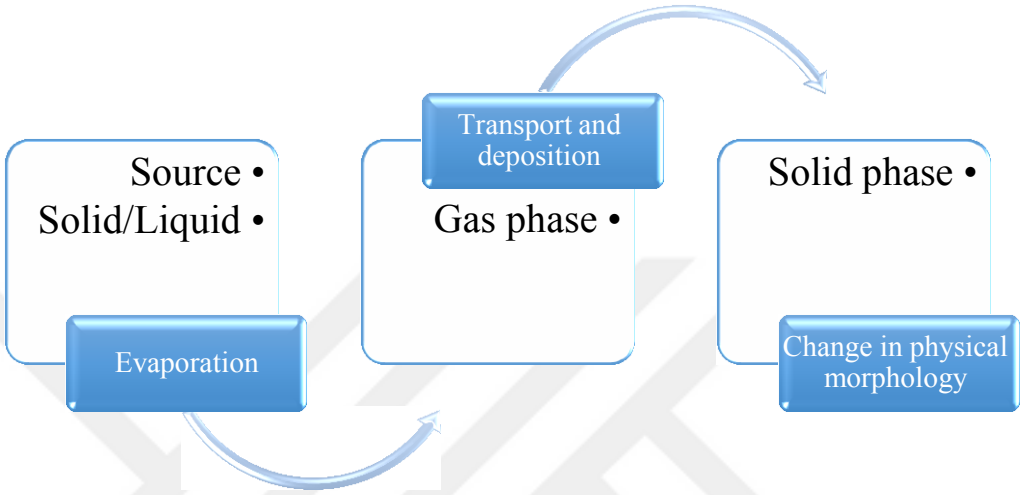

Figure 3.4. Scheme of the morphology of PVD

3.2.1.1. Sputtering

Its classified as a branch of physical vapor deposition PVD, sputtering in physics means the transferring of momentum between active sized particles (noble gas) and atoms on the surface of the target material. In this process a voltage applied between the target and the substrate under vacuum so the target will be the cathode and the substrate is the anode, the applied voltage will help to accelerate the released electron from target, thus the atoms transport from target to the substrate to help thin film formation on the substrate (Seshan, 2001).

3.2.1.2. Pulse Laser Deposition (PLD)

It is belonging to the physical evaporation deposition technique, the pulse of laser is used to evaporate solid materials due to continuous influential of laser radiation, low pulse period and high-power density. A thermal evaporate will lead to release the atoms from a target which is an element, alloys, or compounds. The high purity of this process is one of the most important features. In general, the process involved three steps; the ablation of the target material by a laser beam, formation plasma

plum with highly energetic consist of (atom, molecule, electrons), deposition of material on the substrate (Savale, 2016).

3.2.1.3. Molecular Beam Epitaxy (MBE)

It is one of controlled process for single crystal film or single atomic layer deposition under ultrahigh vacuum UHV (~10^{-11} Pa) qualifications, that generated a beam of molecules or atoms (that does not interact with each other) from more than one source (Knudsen sources or effusion cell which is often cylindrical metallic chamber) (Zehe, 2001). Disadvantages of this process are; an expensive technique, not suitable for mass production, and needing providing UHV condition (Seshan, 2001).

3.2.2. Chemical vapor deposition (CVD)

This technique includes changing in chemical properties of materials besides to phase change. Table 3.1 indicates a comparison between chemical deposition and physical deposition technique. Chemical deposition can be divided into a solution phase and gas phase deposition.

Table 3.1. Comparison between CD and PD deposition technique

Chemical deposition technique	Physical deposition technique
Low cost and wide range of uses materials	More expensive with specific target materials
Suitable for mass production	Limited production
Take place under atmospheric pressure conditions	Carry out under high vacuum conditions HVC
Needed for elevate deposition temperature in the range 100℃ – 800˚C	Lower deposition temperature 200℃ – 500℃
High probability for shattering the substrate	The least probability for substrate smashing

3.2.2.1. Doctor Blade Technique

Doctor Blade (or tape casting) is a widely used method to produce a thin film in a big surface area. It can be work in speed up to several meters per minutes, and it is suitable for coating the substrate for wide area and thickness in several micrometers.

There are two generally different coating devices in use; a rectangular frame and spiral film applicator (Blade et al., 1952).

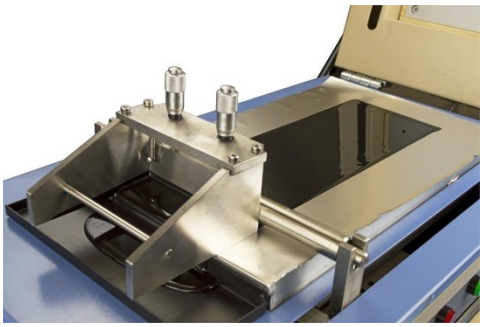

Figure 3.5. Dr. Blade system (Tmaxcn, 1995)

3.2.2.2. Spin-Coating

The spin coating process is one of the various wet chemical thin film deposition techniques. The film thickness this process between (1-200 µm) (Tyona, 2013). An excess amount of solution put on the substrate which is rotated in high speed to separate fluid by centrifugal force.

The spin coating process can divide into four stages: Fluid dispense, Spin-up, Stable fluid outflow (flow controlled), Evaporation dominated drying (evaporation controlled) as shown in Figure 3.6.

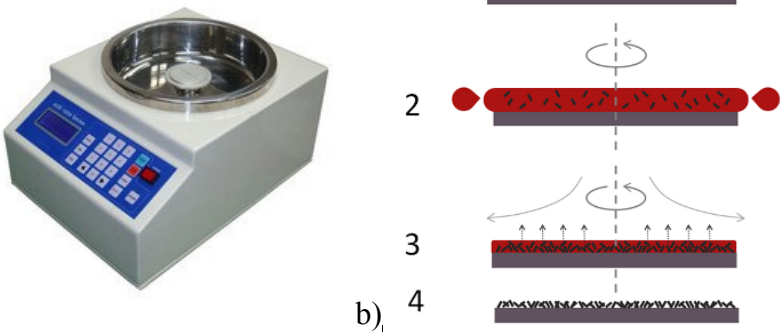

a) b)

Figure 3.6. a) Spin Coating device (IndiaMart, 2018) b) Scheme showed the steps of spin coating (Large Stanford, 2007)

3.2.2.3. Dip-coating

Among the various wet chemical thin film, deposition methods dip coating is used widely. It can be applied uniform film on a flat or cylindrical substrate. Basically, the process may be separated into five important technical stages shown in Figure.3.7; Immersion (dipping), start-up, deposition, withdrawing-drainage, and evaporation.

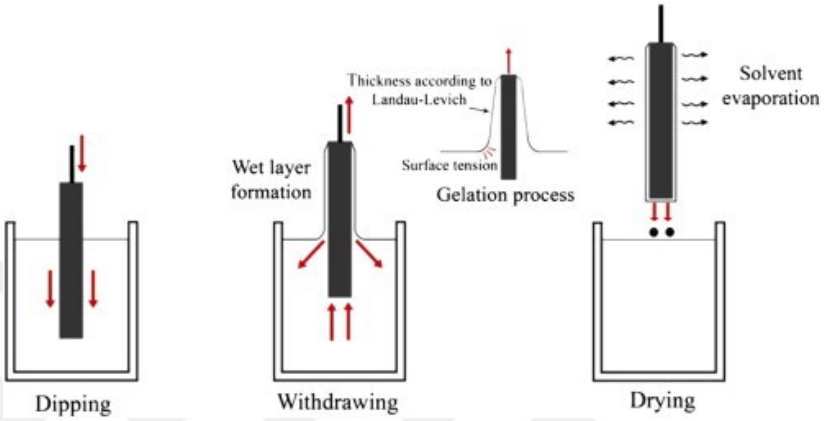

Figure 3.7. Scheme of dip coating stages (Science Direct, 2014)

3.2.2.4. Ultrasonic Spray Pyrolysis (USP) Technique

Ultrasonic Spray Pyrolysis (USP) process depending on electromechanical devices that are vibrating in very high frequency and atomized by passing only when the fluids have low viscosity (Figure 3.8). The advantage of this process; open-atmosphere process, open-reaction chamber, easy access to monitor the deposition, hold adjustment during the experience, formation of multi-layer which is attractive in the manufacture, simple functioning, suitability for atmospheric ambiance production, the ability of large area deposition, the cost of production is cheaper than other techniques.

Figure 3.8. Ultrasonic Spray Pyrolysis system (USP)

USP technique falls within solution - aerosol thermolysis which is produced narrow droplet size (nanosized). Elevated temperature is applied to the liquid droplets atomized of precursors on hot substrates (pyrolysis). The process contains four major stages:

- Dispersion of precursor solution under high-frequency sound wave to destroy the agglomeration in the solution as shown in Figure 3.9.
- Pumping the solution into the nozzle
- Spraying the solution on a hot plate (substrate)
- Formation of the film (in solid phase) from atomizing droplet under atmospheric ambiance or nitrogen gas

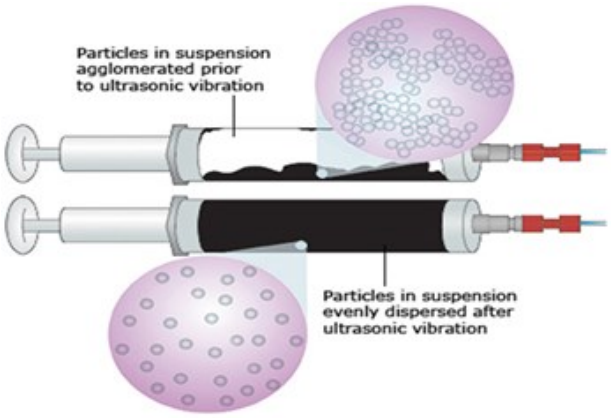

Figure 3.9. Agglomerated particles inside the solution dispersed by ultrasonic vibration (Sono Tek, 2016)

The device included the following units:

1. Ultrasonic spray generator: the unite use to create a high-frequency sound wave with low velocity
2. Syringe pump: the function of this instrument is regulated the flow rate of the precursor solution.
3. Syringe: a tool where a solution is placed and dispersed.
4. Heat plate unite: it's used to heat the substrate up to 600 ˚C
5. Ultrasonic Nozzle with air shaping
6. Temperature regulator: to controls the temperature of the substrate. These are basic apparatus of USP device and there is an extra optional instrument in accordance to the purpose of production.

3.2.2.5. Types of Spray Pyrolysis Systems

There are many types of Spray Pyrolysis Technique. These techniques can be classified according to their energy source, atomizer and nozzle kinds. Such as spray pyrolysis in a tubular reactor SP, vapor flame reactor VFSP, the emulsion combustion method ECM, flame spray pyrolysis FSP, electrostatic and ultrasonic spray pyrolysis USP. Moreover, the second classification which depends on atomizer types can be summarized in Table 3.2.

Table 3.2. Droplet size and atomization rate according to the atomizer (Hamedani, 2008)

Atomizer type	Droplet size (μm)	Atomization rate (cm^2/min)
Pressure	10 - 100	No limit
Nebulizer	0.1 - 2	0.5 - 5
Electronic	0.1 - 10	<2
Ultrasonic	1 - 100	<2

USP is one of that technique which can be used for various materials and such as metals (Au, Ag, Co, Cu, Zn, Fe, Ni), composite oxides (TiO_2, ZnO, AlO_3, RuO_2, CuO, SnO_2, CdS), transparent conductive oxide (ITO, FTO, AZO) and also it can be used in different filed; thin film production, solar cell application, medical, industry etc. It can be used to composing a micron size particle and nanosized particles. The

size of that particles depends on droplet size and the concentration of precursor. In some studies, they found it could control the size of powder by the concentration of precursor. Also, a lot of research mention about the temperature effect (Pingali, Rockstraw, and Deng, 2005), so almost the researches are around the effective parameters on particles size which identifies type and thickness of the film that produced by USP technique. From above its clear that first affected parameter is the droplet size and the second the concentration of precursor and there are other parameters which are discussed in the following paragraph.

3.2.2.6. The affecting factors for USP

In the last period after expansion of thin film deposition technique a wave of research trend to study the parameters that have a direct effect on thin film synthesis. In this paragraph these factors will be summarized:
Modifying precursor of solution and solvent; its play an important role on thin film fabrication and specify the way of the experiment because of its mean controls the concentration of the solution, determining the type of solvent, fixed the quantity of salt that added to the precursor (should be dissolved in the chosen solvent). All these parameters affect the particles size, the probability of cracks on the film surface, structural properties, and thickness of the film. High concentration of precursor solution caused by increased particles size which leads to raising the roughness of the film surfaces, moreover, decreased the pervasion rate because of increase of viscosity (Richner, 2001).

The composition of a solvent; In some cases, need to be added more than one solvent to obtain a good quality of solution and avoid the precipitation which may cause clogging in the pipes of the device. Alteration solvent means different properties of the solution and that lead to change the other factors of the experiment such as deposition temperature, solution flow rate, and concentration. Water, Alcohol, ethanol, methanol, etc., are a suitable solvent for dissolving the materials that used in the USP system. The quantity of all constituents can be calculated by chemical equations (molarity). A study reported the effected of solvent on physical properties of the solution, by using two types of solvent with different boiling point, methoxy-

2-propanol with a low boiling point (120℃) and methoxy-2-propanol by butyl carbitol which has ha igher boiling point (230℃). It was clear that the film with dense morphology deposited by using higher boiling point with higher deposition temperature (Richner, 2001) .

Solution flow rate; It can be organized by syringe pumping that has a wide range of adjustment, the value of it has side effect on thin film formation, and it depends on other factors such as type of nozzle with atomizer, temperature, concentration of solution, diameter of the nozzle, and distance between nozzle and substrate.

Many studies reported the minor effect of solution flow rate, it was used a small value between 1 ml/h to 8 ml/h in electrostatic spray deposition (EDS) process with short distance between nozzle and substrate thus a dump layer formed due to excess of droplet flux that will increase the cracks and stress on the film so the conclusion was; for low value of flow rate the film little denser and less agglomerates than that with higher value (Richner, 2001). That study investigates the impact of solution flow rate depending on distance between nozzle and substrate, in addition, another research in the same field but depending on the temperature of deposition which states; the porosity and structure properties of the film can be directed by chosen the optimum solution flow rate and deposition temperature; applying lower flow rate with low temperature the film will be in the powder form because incompletely reaction, and not sufficient activation energy, on the contrary in high value (T > 500 ˚C, solution flow rate > 0.9 ml/min) the film will be in agglomerate pours form because of the limited time for droplet to pervade on substrate, and huge quantity of deposited droplets (Hamedani, 2008).

Substrate temperature; to control and determine the nature of a thin film; temperature has a direct impact on the formation of the film structure, roughness, etc. According to the physical law when the temperature increased that make the particles far away from each other and the pores also increase. This fact going to be the key to controllable the nature of the thin film surface texture. It will be able to synthesize a compact layer or porous by playing with this factor. In a study reported the effected

of substrate temperature on thin film morphology by using EDS. It was observed that below 200 ˚C a damp layer will formed upper the film during deposition so that create a cracked layer because of strain impact, while in high temperature (> 350 ˚C) all spray droplets are dry and it will be formed as a separately which is lead to increase the roughness of the film and created a dense films (Richner, 2001) . Another investigation notified the temperature deposition influence; at low temperature > 300 ˚C the droplets will tarnish the surface because it still rich with solvent, in that case, a need for annealing the film to boost the crystal formation, on the other hand, increased the temperature to 500 ˚C make separate solid particles formed upper the film with many pores due to evaporating all the solvent (Hamedani, 2008).

The distance between substrate and nozzle: It is another parameter can be used to regulate the layers of film formation and has main influence in thickness of film, morphology, and distribution of particles on the substrate. The value of it can be determined mathematically depending on the type of nozzle, deposition area, and other parameters, thus there are a limited range for that distance depending on the type of atomizer and substrate size thus selected the suitable rang essential to not loses the atomized particles due to the high temperature of deposition.

The distance between nozzle and substrate effect also announce by Hamedani, Hoda Amani et al 2008, different distances were tried in the range of 3 to 8 cm, when the distance so small that will lead to formed a thick layer on substrate while the particles scattered on surface and look like powder form in rather long distance, in addition far distance there will be an exhaustion for spray particles thus the important point here is that distance can be determined according to deposition process and other factors.

Time of deposition: It is one of the major influential factors in film morphology; structure properties, thickness, and roughness. According to the physical laws when the cycles count and time of deposition increase that means rapid deposition with

aggregated of droplets on a substrate which leads to decrease the strain of layers leading to cracks and raised the roughness.

In 2001 an investigation documented the effect of increasing the time of deposition on the thin film structure. Thin film thickness was increased after 45 min, in addition, the film becomes porous with particles agglomerates after 300 min because of slowly pervade of droplets on a substrate which create separated particles and increased the roughness (Richner, 2001).

4. PRODUCTION AND CHARACTERIZATION TECHNIQUES

4.1. Introduction

In this chapter the thin film deposition experiment conditions and parameters will be discussed where Zinc doped titanium dioxide thin film was deposited on glass substrate by ultrasonic spray pyrolysis ((USP) SONO-TEK Flexi, USA) technique. After that, the dye-sensitized solar cells were produced with the same technique with the substrate temperature at 300 ˚C. The surface morphology investigated by scanning electron microscopy (SEM) (FEI Quanta FEG 250, EU), Energy Dispersive X-Ray Spectroscopy (EDS) coupling with SEM was used to element analysis and chemical characterization, the structural properties study with X-ray diffraction (XRD) (Bruker D8 Advance Twin-Twin, EU), surface topography investigated with Atomic force microscopy (AFM) (Nano Magnetics, TURKEY). UV-measurements was taken by UV- visible spectroscopy. The electrical properties for the dye solar cell investigated by Current-Voltage measurement system (Keithley 2400, Tektronix). The details of experimental conditions and parameters will be discussed in the following paragraphs.

4.2. Thin Film Production

4.2.1. Substrate cleaning

There are many methods of cleaning which are using different kinds of chemical solvent and solution. There are a few wet chemicals cleaning such as alkaline cleaning which is used to remove oils, grease, wax, and various type of particles from metallic surface, solvent cleaning to remove organic soils, oil, grease, acid cleaning to remove light oxides from metal surface, emulsion cleaning uses organic solvents (oils) dispersed in an aqueous solution to clean non-metallic part, Ultrasonic clean that used high frequency 20 - 45 KHz, moreover there are dry cleaning procedures. In this work wet chemical cleaning procedure was used in the following steps:

- The glass washed by detergent to remove the dust particles; rinsed by water; and then rinsing by deionized water DI, drying with nitrogen.

- The glass substrates were soaked in DI water and placed in the ultrasonic device for cleaning under 40℃ for 25 min
- It has been output from device washed by DI water drying with nitrogen
- After that it was soaked in a mixture of Ethyl alcohol; Acetone; and Isopropyl alcohol placed again in the ultrasonic device under 40℃ for 25 min
- It is output from the device washed by DI water drying with nitrogen; then washed by Ethanol and drying with nitrogen.

4.2.2. Precursor Solution Composition

The precursor solution was prepared from mixture of 0.1 M of titanium(IV) bis acetyl acetonate diisopropoxide [$(Ti(Ac)_2(IP)_2][C16H_{28}O_6Ti$] and dissolved in pure ethanol 50 ml Zinc acetate dihydrate [$(CH_3COO)2Zn.2H_2O$] was added as a dopant with 8 at.%, then placed it in ultrasonic device to dissolve the solid particle of solution for 1h, under 30 ˚C. Zinc-doped titanium dioxide thin films were deposited on glass substrate by ultrasonic spray pyrolysis (USP) with substrate temperature 300˚C

4.2.3. Ultrasonic Spray Pyrolysis preparation

After substrate cleaning and precursor solution composing, USP deposition device will be adjusted with the following parameters: the air shaping 2 KPa, substrate temperature at 300 ˚C, nozzle temperature at 50 ˚C, motor cooling 3 psi, nozzle cooling 25 psi, nozzle frequency at 120 KHz, solution flow rate at 0.5 ml min^{-1}. The distance between the substrate and the nozzle was 8cm. For each cycle count which is 25, 50, and 75 correspond to 8, 16, and 25 ml respectively (cycle time ~ 0.62 min). The experiment was held in an open reaction chamber and open atmospheric ambiance with nitrogen gas pumping to dry the humidity of the air. These parameters play a critical role in thin film structure, physical, chemical and optical properties, thickness, crystal orientation, etc., the influence of these factors were discussed in details in chapter 3 (3.3.4).

4.2.4. Annealing

The deposited Zn:TiO_2 thin film samples were annealed in the oven up to 550℃ for glass substrate and 470℃ for ITO glass; the annealing was applied gradually to protect the samples from damage. The important thing about annealing is to modify the crystal orientation of the film in addition; we noticed the color change of samples.

Figure 4.1. Photo of the oven which annealing held under atmosphere.

4.3. Thin film characterization

4.3.1. Scanning electron microscope (SEM)

FEI Quanta FEG 250, EU (SEM) system which can be seen in Figure 4.2 was used to characterize the surface morphology of samples, thickness, grain size, and effect of annealing, and deposition parameters on the film morphology.

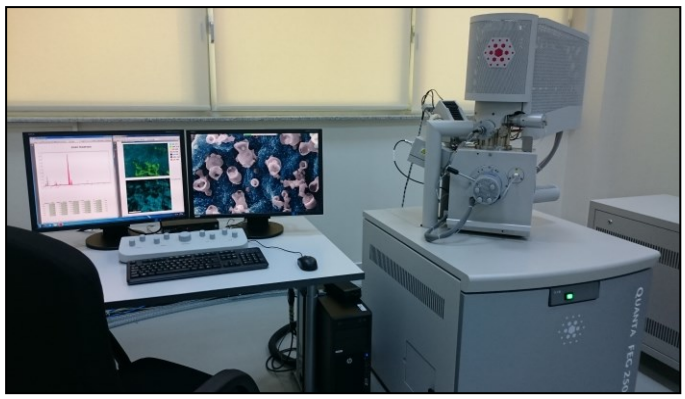

Figure 4.2. Scanning electron microscope system (SEM)

The electron beam produced at the top of the microscope by an electron gun (FEG gun), electron beam transmitted vertically in a vacuum and accelerated by the anode. The beam travels through the electromagnetic field, the lenses focus electron beam down towards the sample, a mechanism of deflection coils enables to guide the beam so that it scans the surface, when the beam hits the sample that produces: secondary electron (SE), backscattered electron (BSE), X-ray, a detectors collect these (X-ray, SE, BSE) and convert them in to a signal that is sent to screen to produces final image (Cotutelle et al., 2013).

4.3.2. Atomic Force Microscope (AFM)

Nano Magnetics (Turkey) Atomic Force Microscope (AFM) which is shown in Figure 4.3 was used to create the 2D and 3D images of the thin film surfaces. It has wide commercial and scientific application, using for surface topography analysis various types of surface materials conductors, semiconductors, and insulators; for that reason There are several types of operation modes categorized depending on the kind of force that generated between the sample and the tip, the cantilever pulls on the sample surface this means the probe in touch with sample that mode called static mode, while in dynamic mode there is no touching between the probe and surface of sample the tip will approach from the sample. When the tip approaching from the sample a force generated between the tip and the surface of the sample leads to deflection in cantilever submit to hawk force; that can be measured by deflection in laser beam on fixed mirror, the reflex laser beam monitors online matrix of photodiode, also we can measure the deflection in other ways such as optical interference and by use pesos electric but, the deflection in laser beam more accurate (Harjee, 2011).

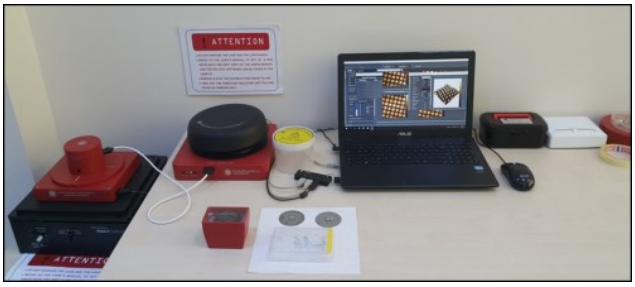

Figure 4.3. Atomic Force Microscope (Nanomagnetics ez-AFM)

4.3.3. X-Ray Diffraction (XRD)

Bruker D8 Advance Twin-Twin X-Ray Diffraction (XRD) system was used to study the structural properties of the samples. XRD one of the most important process that belongs to the non-destructive technique. It is used to characterize structure properties, crystal orientation, phase configuration, and defects.

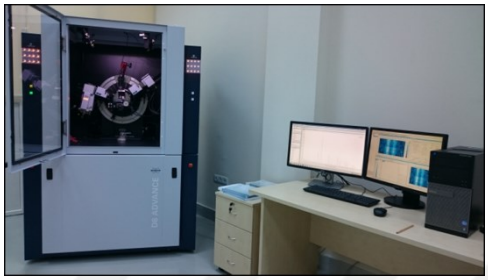

Figure 4.4. X-Ray diffraction (XRD) system (Bruker D8 Advance Twin-Twin)

4.3.4. Bragg's law

Atoms organized in uniform layers each of theme called atomic plane, the distance between theme fixed which is d and monochromatic beam of wavelength l oncoming to *d* that beam fallen on the atomic plane with angle θ, if the path difference between two neighboring atomic planes was equal to the wavelength of a fallen beam that will lead to positive interaction as shown in Figure 4.5. That difference is given by $2d \sin\theta$ only when the incident and the diffracted angle is equal, thus, the condition can be written as the following equation for all crystalline solid materials (Hamedani, 2008):

$$n\lambda = 2dsin\theta \quad (4.1)$$

Where:

n integer number

λ wavelength of X-ray

d distance between atomic layers

2θ Bragg's angle

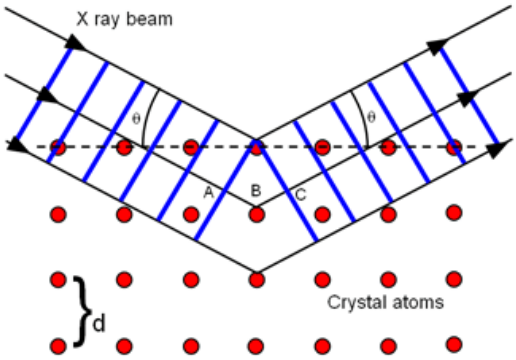

Figure 4.5. X-ray diffraction (Teaching Advanced Physics, 2018)

4.3.5. X-ray diffraction pattern

The pattern includes the relationship between 2θ and the intensity for different value of incident angles. Much information can be obtained from that pattern such as: by comparing the obtaining pattern with international center for diffraction data ICDD can identify composition of crystalline, the laying atom, lattice parameter, and unit cell size can be obtained from d position, to appraise the atom type intensity values are used, full width at half maximum FWHM employ to identified crystal size and microstrain of the sample, and 2θ can be used to determine the inter planer atom (Cotutelle et al., 2013).

4.3.6. UV-vis spectrophotometer

UV - spectrophotometer was used to study the optical properties of the thin film. The ultraviolet photons in the range of (200 - 400 nm) and the visible photons (400 - 800 nm) wavelengths. It is one of the electronic spectrometers which depends on a simple principle that is a photon of incoming radiation excited an electron; moreover; a spectrometer studies the interaction between molecules and ultraviolet-visible radiation.so after interaction an electronic transition will occur from low energy level to higher level, Figure 4.9. involve the electronic transition, to make the system back to the ground state there are two way either emission or reflectance.
The energy of the system can be determined by the following equation:

$$\Delta E = h\nu = \frac{hc}{\lambda} \quad (4.2)$$

Where ν is the frequency of the electromagnetic radiation, c is the speed of light in vacuum and λ is the vacuum wavelength (Förster, 2004).

The important information that can be obtained from UV - vis spectroscopy are the energy gap, absorption, and wavelength of absorbed light (Kumar, 2006).

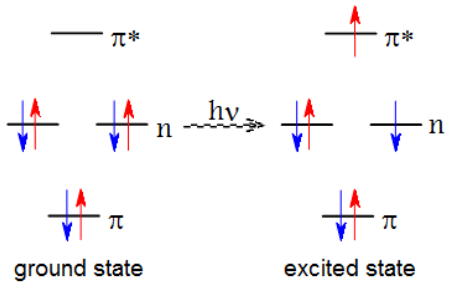

Figure 4.2. Electronic transition by photon energy (UcsbEdu, 2012)

4.4. Device Production

Dye-Sensitive Solar Cell DSSC was produced by the following steps after cleaned the ITO glass substrates with wet chemical methods:

- Zn (8 at. %) doped TiO_2 deposited on ITO glass substrate with 250 ˚C by USP system with fluid volume 8 ml and 16 ml as shown in Figure 4.10, annealed up to 470 ˚C

a) 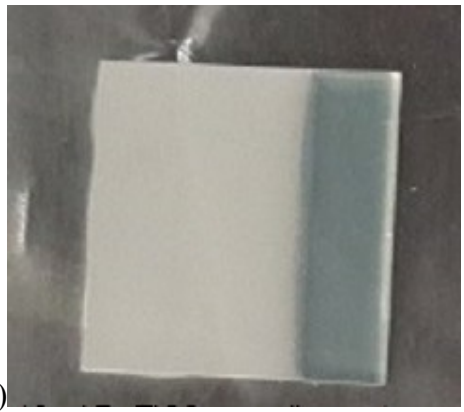 b) 

Figure 4.3. Zn doped TiO_2 on ITO glass substrate annealed up to 470 ˚C

- The film soaked in Ru ruthenium (II) dye $C_{58}H_{96}N_8O_8RuS_2$ which was prepared by dissolved 1.2 mg of solid dye in 10 ml of liquid acetonitrile CH_3CN. Figure 4.11
- The second substrate of ITO glass used as an anode after covering it with graphite
- The two substrates stick together, then the electrolyte that contains 0.83 g of Potassium Iodine KI, 0.12 g Iodine I_2 and 10 ml of Ethylene glycol $C_2H_6O_2$ has been injected between the substrates. After that, we started with electrical measurements as shown in Figure 4.12.

a) 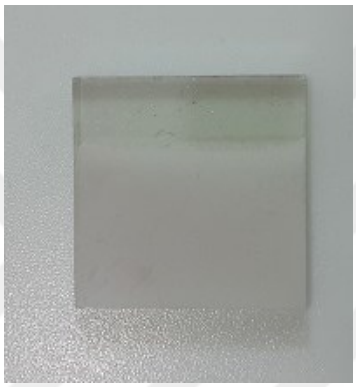 b) 

Figure 4.4. a) Photo of 16 ml of Ru – Zn doped TiO_2 B) 8 ml of Ru - Zn doped TiO_2 on ITO glass was soaked Ru ruthenium (II) dye $C_{58}H_{96}N_8O_8RuS_2$

a)  b) 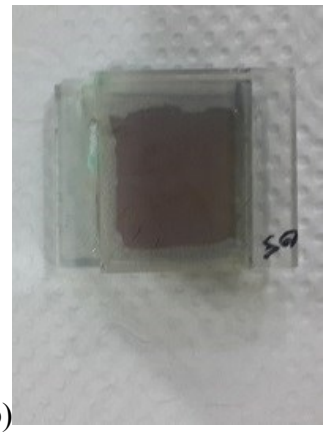 c) 

Figure 4.5. a) Before electrolyte injection b) KI electrolyte injected and c) current-voltage measurements under light/dark

5. RESULT AND DISCUSSION

In this chapter we will display the result that we obtained it from XRD diffraction technique used to study structural properties of our film, surface topography analyzed by AFM, and the surface morphology of the samples searching by SEM, EDS which coupling with SEM was used to element analysis and chemical characterization, UV-measurements was taken to calculate the band gap, and the electrical properties for solar cell device that obtained from Current-Voltage measurement system; all these measurement results will be discussed in the following paragraphs.

5.1. Structure Properties XRD Measurement

As can be seen in the XDR Figure 5.1 that, the peak of intensity appears after annealing the sample. The main peak becomes narrowing; sharping when the temperature increase, the results showed that the Anatase TiO_2 peak appears after annealing the samples at 400 ˚C. The crystal size of the thin films increased from 116 Å to 505 Å by increasing the annealing temperature from 300 ˚C to 550 ˚C that for the same sample which is 25 ml deposition as showing in Table 5.1. In other hands we compared the result for different precursor solution volume and we've got similar result to that of various temperatures that mean increasing of cycles count has no effect on crystal size but it can be used to increase thickness film; the crystal size starting from 151 Å, 161 Å, 155 Å for 8 ml, 16 ml, 25 ml sequentially for annealed samples as shown in Figure 5.1, and given in Table 5.2. The increasing of crystal size is due to the extending in unit lattice parameter, which is caused by enough temperature of annealing.

Table 5.1. The crystal size for different fluid volume (annealed up to 550 ˚C

Fluid volume (ml)	Color	FWHM	Crystal size D (Å)
8	Black	0.598	151
16	Green	0.561	161
25	Red	0.255	155

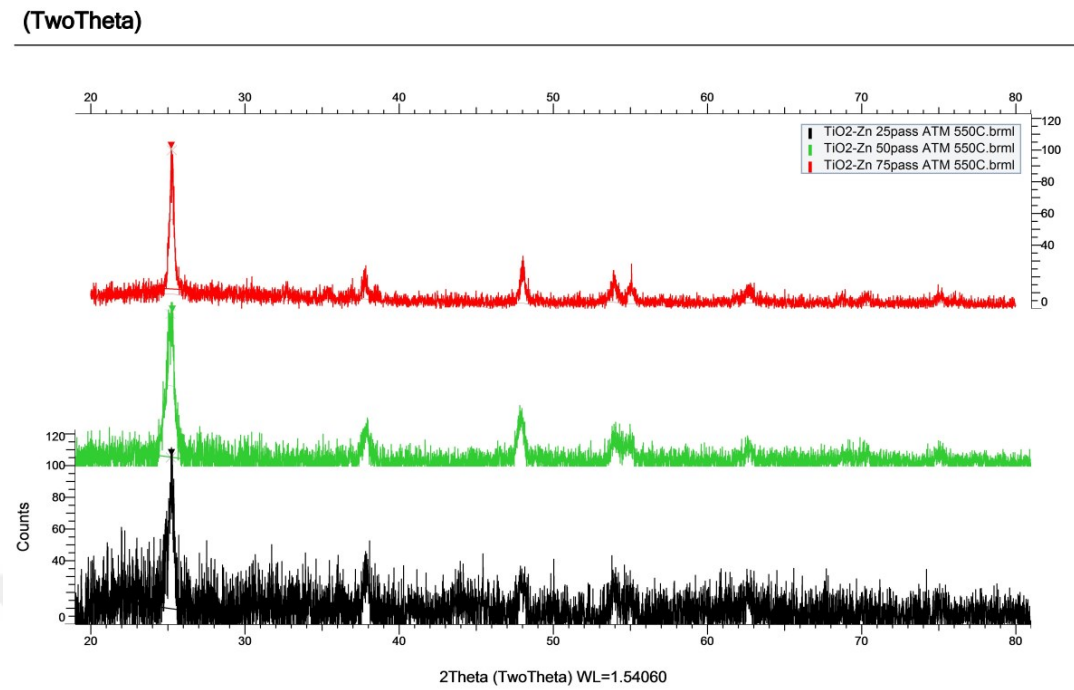

Figure 5.1. Patterns of Zn-doped TiO_2(8 at. %) for 8 ml, 16 ml, and 25 ml deposition volumes annealed up to 550 patterns of Zn doped TiO_2 (8 at. %) for 8 ml, 16 ml, 25 ml deposition volumes annealed up to 550 ˚C

It can be seen that, the mean structure of our films is tetragonal of Anatase (66.7%) TiO_2 with unit cell parameter a = b = 3.78520 Å, c = 9.51390 Å, there are also Rhombo.H.axes (9.6%) $ZnTiO_3$ Zinc Titanium Oxide Ecandrewsite, that has unit cell parameter a = 5.07870 Å, c = 13.92700 Å, c/b = 2.74224 a = 8.42900 Å, a/b = 1.00000, c/b = 1.00000 for Zn_2 TiO_3O_8 Zinc Titanium Oxide cubic phase (22.6%), and TiZn titanium Zinc in cubic form (1.1%) were a = 3.15000 Å as shown in table 5.3. These differences in crystal phases are due to dopant atoms, the way that take their positions in the lattice, and doping procedure. The crystallite size D is calculated by using the Scherrer equation (Khairy and Zakaria, 2014):

$$D = k\lambda/\beta cos\theta \qquad 5.1$$

Where k = 1is the shape factor, λ is the X-ray wavelength of *CuK*α radiation $\lambda_{CuK\alpha} = 1.5406$ Å, β is the full width of diffraction line at half of maximum intensity (FWHM) and θ is Bragg's angle.

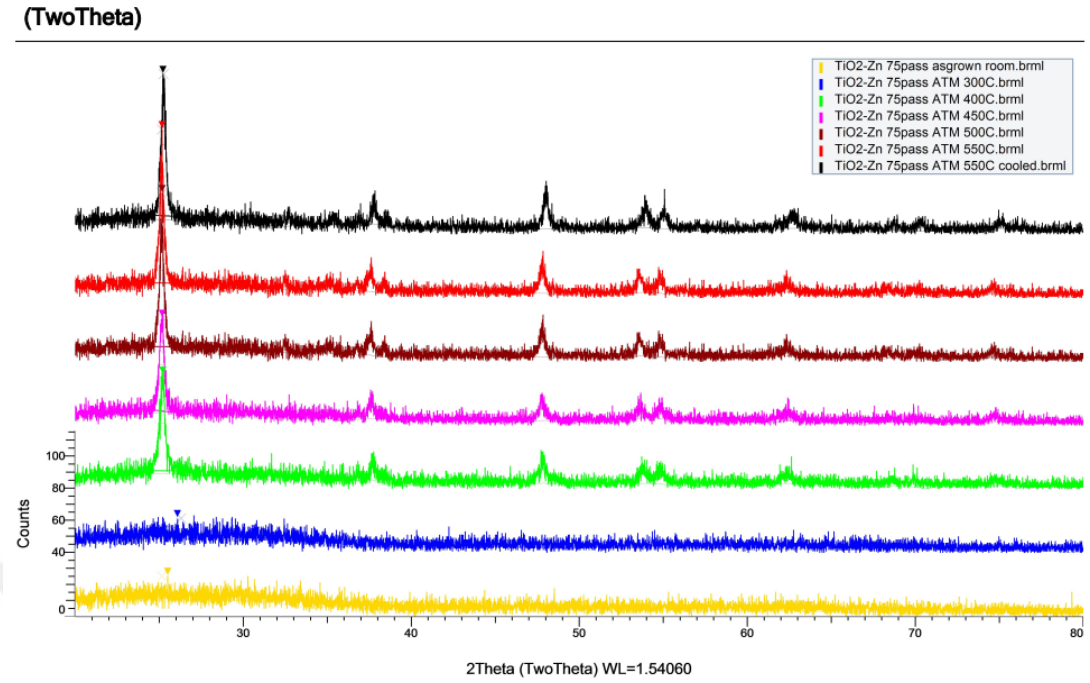

Figure 5.2. XRD pattern of Zn doped TiO_2 (8 at. %) annealed at different temperatures start from (300 ˚C to 550 ˚C sequentially)

Table 5.2. The relation between annealing temperatures for (25 ml sample) and crystal size D

Annealing temperature (˚C)	**Color**	**FWHM**	**Crystal size D (Å)**
300	Blue	0.775	116.9
400	Green	0.309	292.3
450	Pink	0.284	318.0
500	Brown	0.209	439.9
550	Red	0.179	504.9

Table 5.3. Crystal lattice parameters

Lattice	**Concentration level**	**S-Q %**	**Crystal plane**	**a=b (Å)**	**c (Å)**	**z**	**Formula**
Tetragonal	Major	66.7	101	3.78520	9.51390	4	TiO_2
Rhombo. H. axes	Major	9.6	003	5.07870	13.92700	6	$ZnTiO_3$
Cubic	Major	22.6	220	8.42900			Zn_2TiO_8
Cubic	Trace	1.1	100	3.15000		1	TiZn

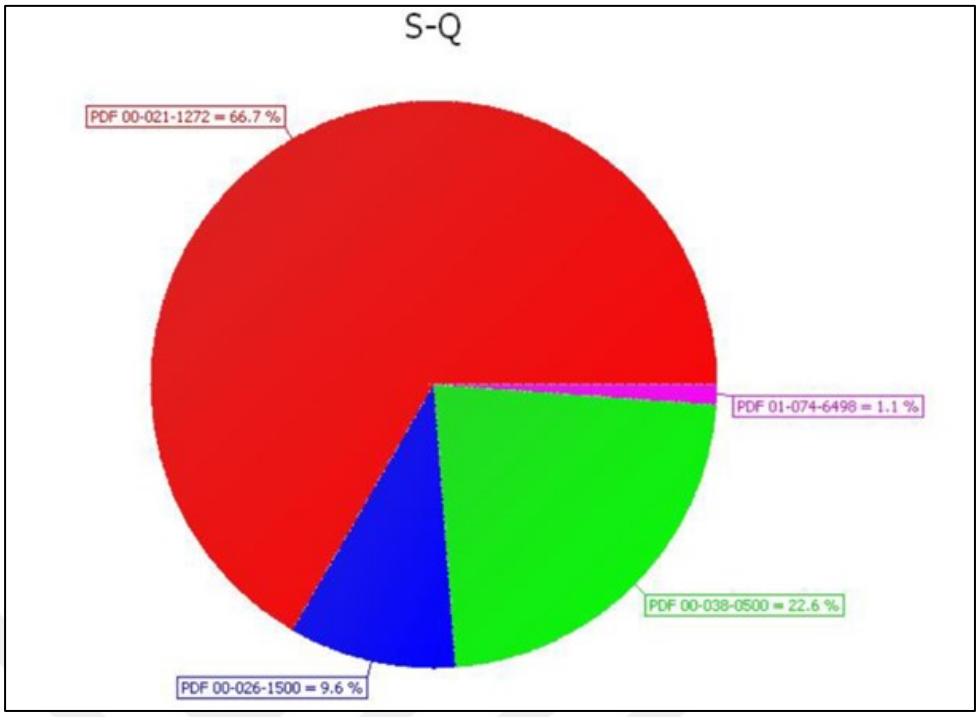

Figure 5.3. S-Q represent to the ratio of crystal of the TiO_2 film

Pie chart representation of the Semi quantitive analysis showed that; (S-Q) for PDF 00-021-1272 = 66.7% TiO_2 Anatase (red), PDF 00-026-1500 = 9.6% $ZnTiO_3$ Ecandrewsite (blue), PDF 00-038-0500 =22.6 Zn_2TiO_8 Zinc Titanium Oxide (green) and PDF 01-074-6498=1.1% TiZn Titanium Zinc (pink).

XRD pattern in Figure 5.3 shows the diffraction peak of Anatase TiO_2 (annealing sample) in red color PDF 00-021-1272, while PDF 00-026-1500 for $ZnTiO_3$ in blue color, in green color PDF 00-038-0500 belong to $Zn_2Ti_3O_8$ and TiZn in pink color PDF 01-074-6498.

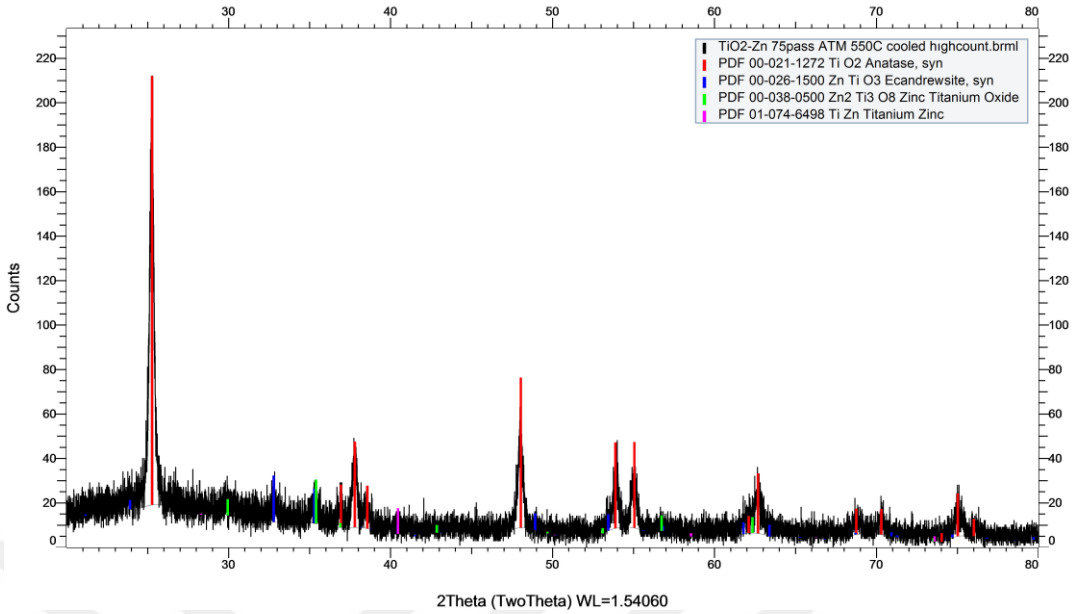

Figure 5.4. XRD pattern of Zn dopant TiO_2 annealed up to 550 ˚C

5.2. Surface Morphology of the Films (SEM)

The surface morphology of the samples was characterized by SEM under low vacuum (30 Pa). The image showed the spherical shape of microcrystals of Anatase TiO_2 as shown in Figure 5.4a and the film becomes more uniform with dense morphology after annealed it's up to 550 ˚C as shown in Figure 5.4b. in some images exhibit the bulk particle of microspherical TiO_2 Figure 5.4a. After annealing grain size in the range 20 nm to 55 nm and the bulk particles disappear that due to the grain boundary movement that happened because of harmony between the neighboring grains by removing their common boundaries. The image exhibits the porous nature of the film Figure.5.4c, d, which mean increasing the active area that is making it suitable for fabrication of DSSC. The cracks appear after increased fluid volume up to 25 ml (increased the fluid volume) as shown in Figure.5.4e, because of the perpendicular high of thickness make the strain of the film decreased which is make the cracks appeared, the size of that cracks increase after annealing Figure 5.4e. Therefor suitable thickness for our film less than 25 ml means less than (400 nm) as shown in Figure 5.5.

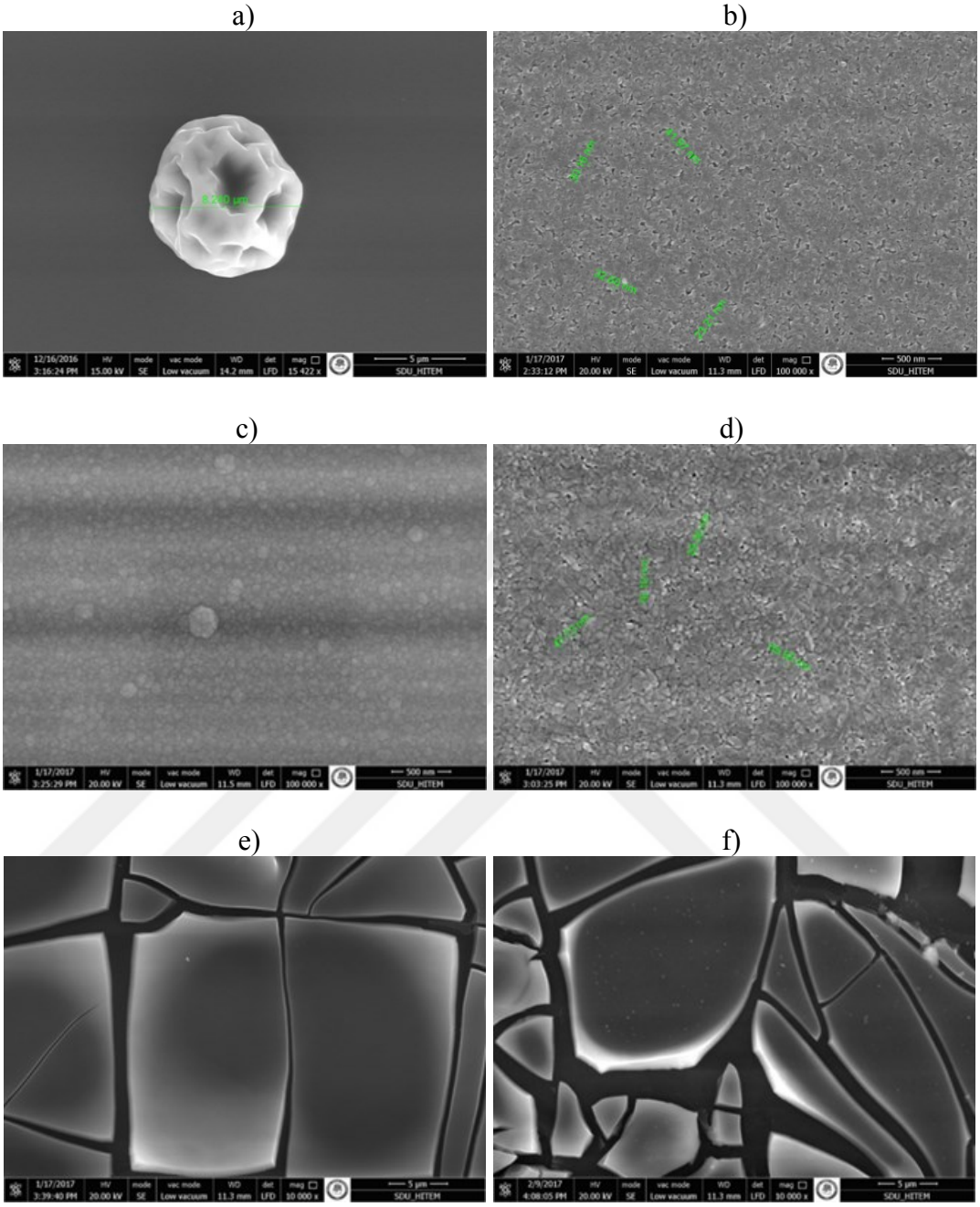

Figure 5.5. SEM images of (a) 8 ml for as-grown sample (b) 8 ml annealing (550 ˚C) (c) 16 ml for as-grown (d) 16 ml annealing sample (e) 25 ml for as-grown (f) 25 ml annealing sample

The images obtained in Hydrogen Technology Research and Application Center (HITEM) laboratory under low-vacuum mod and high acceleration voltage in between HV 10 – 30 KV.

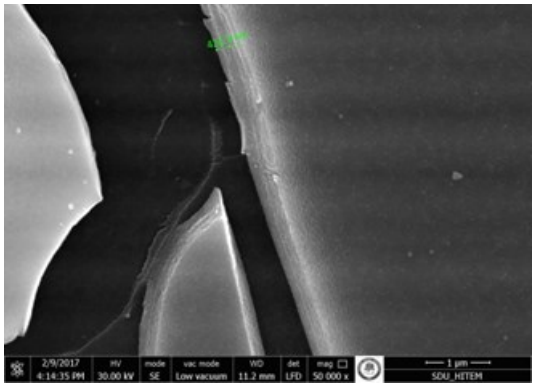

Figure 5.6. The thickness of 25 ml ~ 420 nm thin films after annealing up to 550 ˚C

SEM images exhibit TiO_2 nanoparticles spherical shape with some concavity Figure.5.6a these holes appear because of returning of vapor to the liquid stoke of the solution after condensing hastily and surprisingly due to the high deposition temperature which makes particles shrink in certain areas. The size of concavity about 2.4 µm after annealing as shown in Figure 5.6.

a) b)

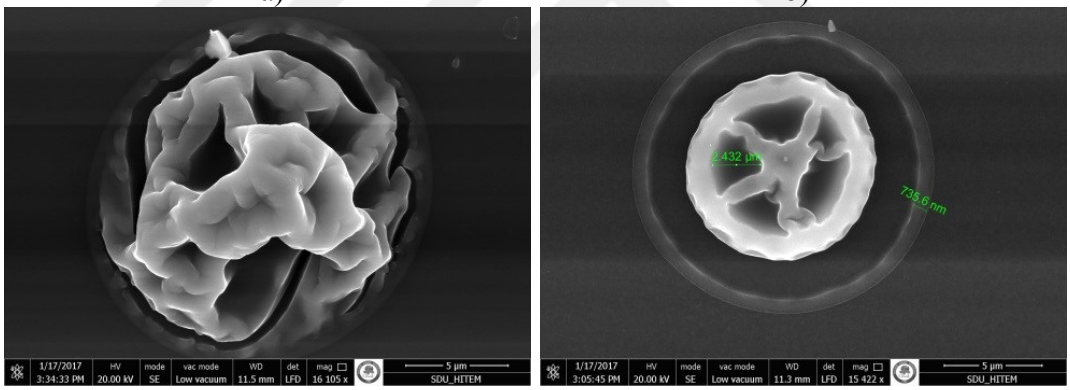

Figure 5.7. SEM images for 16 ml (a) TiO_2 microparticles spherical shape with some concavity (b) size of concavity about 2.4 µm after annealing

Energy Dispersive Spectroscopy EDS analysis has used a coupling with SEM to element analysis and chemical characterization for a different area and the result was so appropriate with theoretical calculation moreover, there is no change in elements weight, the atomic percentage for all samples before and after annealing. The result exhibits a high atomic percentage of Oxygen that because the experiment was done in open atmospheric chamber moreover, the high percentage error value for Zinc analysis is due to the ratio of doping.

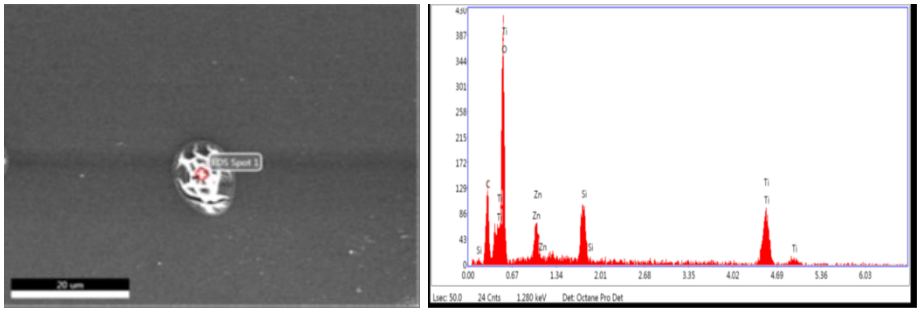

Figure 5.8. EDS result for element analysis 8 ml as-grown sample

Table 5.4. Involving the composition of elements, weight and the atomic percentage of 8 ml as-grown sample

Element	Weight %	Atomic %
OK	38.06	52.00
ZnL	5.31	1.87
TiL	36.89	16.83

For annealing sample, there is no Sharp change in element analysis which is a logical result and if there is a little different that's attributed to the percentage error and chosen area of the sample. The result is shown in Figure 5.8 and explains in Table 5.5.

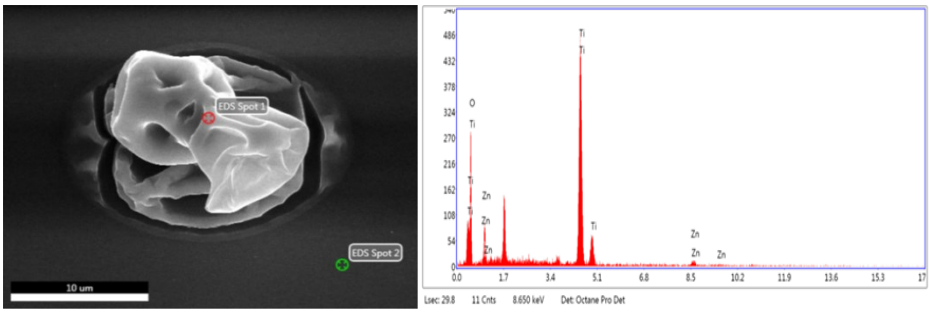

Figure 5.9. EDS result for element analysis 8 ml annealed sample

Table 5.5. Explain the composition of elements, weight and the atomic percentage of 8 ml annealed sample

Element	Weight %	Atomic %
OK	53.42	77.85
TiL	42.59	20.73
ZnL	3.99	1.42

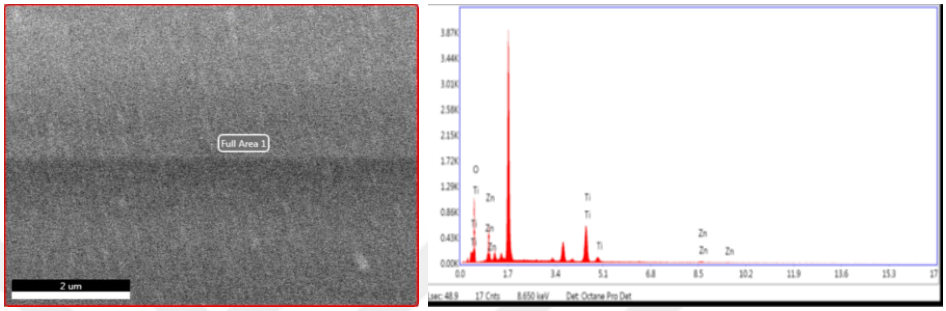

Figure 5.10. EDS result for element analysis 16 ml as-grown sample

Table 5.6. Involving the composition of elements, weight and the atomic percentage of 16 ml as-grown sample

Element	Weight %	Atomic %
OK	69.26	87.37
TiL	27.89	11.75
ZnL	2.85	0.88

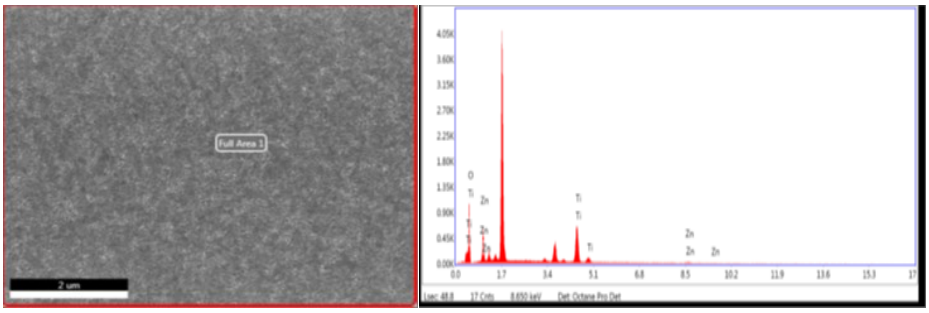

Figure 5.11. EDS result for element analysis 16 ml annealed sample

Table 5.7. Involving the composition of elements, weight and the atomic percentage of 16 ml annealed sample

Element	Weight %	Atomic %
OK	69.12	87.29
TiL	28.61	12.06
ZnL	2.27	0.70

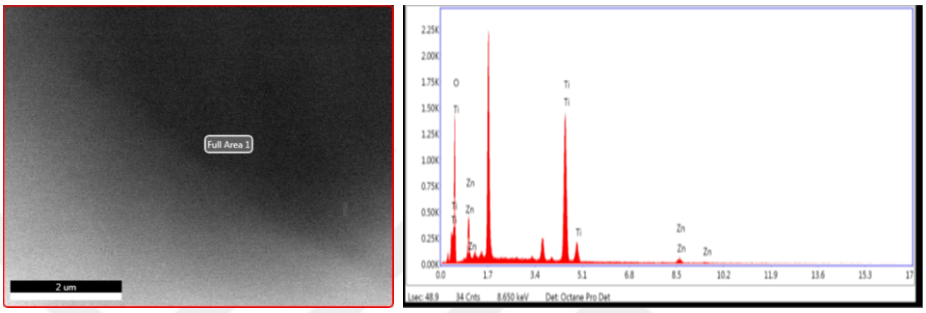

Figure 5.12. EDS result for element analysis 25 ml as gown sample

Table 5.8. Involving the composition of elements, weight and the atomic percentage of 25 ml as-grown sample

Element	Weight %	Atomic %
OK	60.58	82.64
TiL	34.54	15.73
ZnL	4.88	1.63

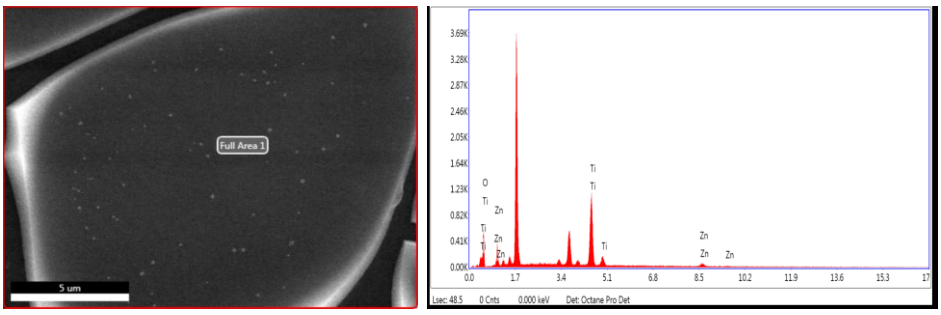

Figure 5.13. EDS result for element analysis 25 ml annealed sample

Table 5.9. Involving the composition of elements, weight and the atomic percentage of 25 ml annealed sample

Element	Weight %	Atomic %
OK	68.31	86.95
TiL	28.01	11.91
ZnL	3.68	1.51

5.3. Surface Topography Measurements (AFM)

AFM was used to measure the surface roughness of the films. The image of Zn-doped TiO_2 showed that the film is porous with small pinholes, so that is completely harmonized with SEM result. The film roughness is 4.10 nm, its decreased to 1.16 nm for 8 ml after annealing which can be seen in Figure 5.13 a and b. For 16 ml deposition, it lowers from 7.47 to 1.40 nm as can be seen in Figure.5.14 a and b. Moreover, 15.13 nm becomes 3.51 for 25 ml deposition which is shown in Figure 5.15 a and b. The 3D image of the films shows the mountains and valleys like formation. The sample was annealed up to 550 ˚C which makes the roughness decreased, as it mentioned and it's become homogeneous, smoother than as-grown film. After annealing, the voids disappear that was obvious from XRD rustle which is apparently increasing of grain size. The roughness of the film played important role in determining the electron transport behavior if the Zn-doped TiO_2 use as a compact layer in perovskite solar cell. The different fluid volume means a change in film thickness so it is obvious that 8 ml thickness is not suitable for used parameters such as annealing temperature and solution concentration in other cases using elevated temperature of annealing require increase solution volume to make it proportional with that temperature. The image of 25 ml showed some defect that because of many reasons such as substrate scratches which may occur during the cutting and cleaning procedure. Table 5.10. explain the changing of roughness with fluid volume before and after annealing.

Table 5.10. The changing of roughness with fluid volume before and after annealing

Fluid volume (ml)	Roughness (before annealing) (nm)	Roughness (after annealing) (nm)
8	4.10	1.16
16	7.47	1.40
25	15.13	3.51

a)

b)

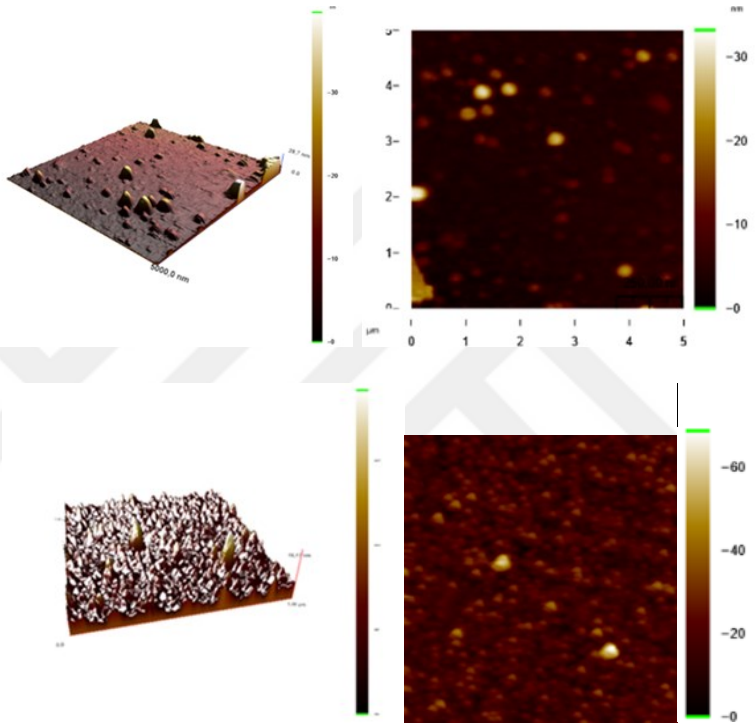

Figure 5.14. Image of Zn-doped TiO_2 8 ml (a) 3D and 2D image as grown with roughness R_a= 4.10 nm (b) 3D and 2D image annealing with roughness R_a = 1.16 nm

a)

b)

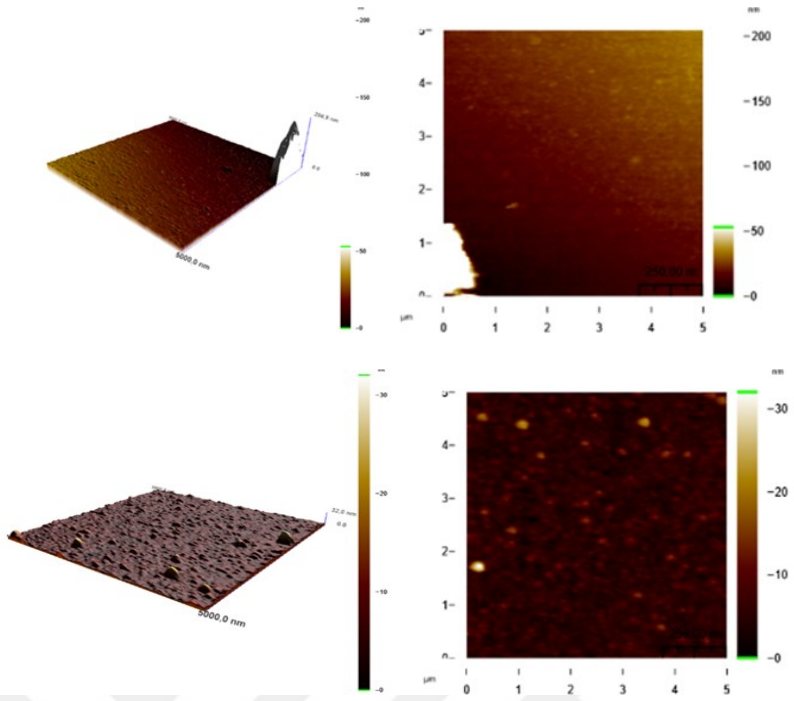

Figure 5.15. Image of Zn-doped TiO_2 16 ml (a) 3D and 2D image as grow with roughness R_a = 7.47 nm (b) 3D and 2D image annealing with roughness R_a = 1.40 nm

a)

b)

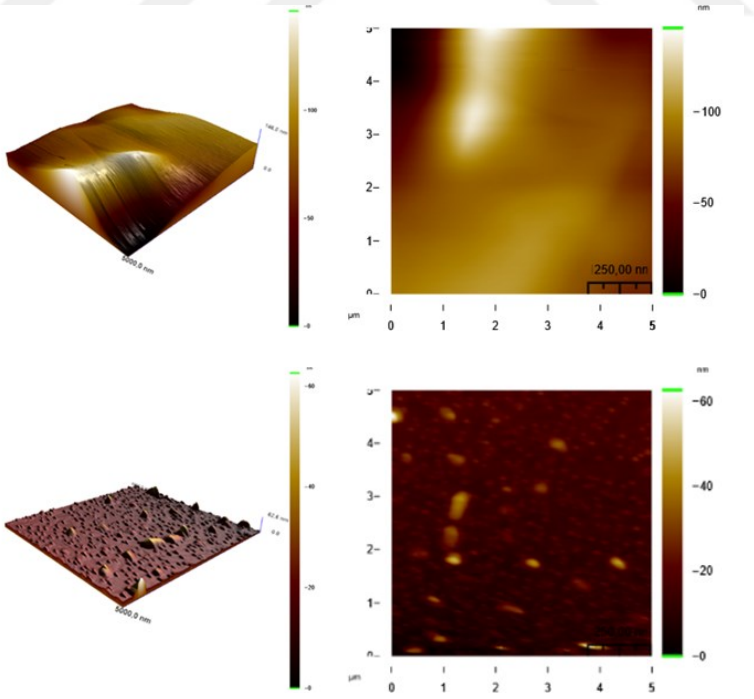

Figure 5.16. Image of Zn-doped TiO_2 25 ml (a) 3D and 2D image as grown with roughness R_a = 15.13 nm (b) 3D and 2D image annealing with roughness R_a = 3.51 nm

5.4. Optical Properties UV Measurement: Optical Properties

UV-vis spectroscopy was used to measure the optical absorbance spectra and optical bandgap value of the films. The results refer that the higher absorption below 350 nm, that means the band gap value increased after Zn doping compared to the theoretical results which suggest that E_g of TiO_2 ~ (3.0 - 3.2 eV). To calculate bandgap it can be used the equation: ($E_g = hc/\lambda$) (Khairy and Zakaria 2014) as well as, E_g = 3.82, 3.78, and 3.78 eV for 8 ml, 16 ml, and 25 ml as grown respectively while for annealed samples there is no marked change in band gap values, E_g = 3.84, 3.76, and 3.72 eV for 8 ml, 16 ml, and 25 ml sequentially as shown in table 5.11 and 5.12. At previous works the wide bandgap of TiO_2 decreased after metal doping; for different Zn concentration (1.0, 3.0, 5.0, and 7.0 mol) the band gap decreased and became (3.25, 3.73, 3.72, 3.58, and 3.26 eV) sequentially (Wu et al., 2016), other study compared between pure and Zn-doped TiO_2 the result is as expected diminution of bandgap with doping and shifting the absorption to red region (Khairy and Zakaria, 2014). In our work the comparison was between different fluid volume and the effect of annealing for the same Zn concentration (8 at. %), there is very small shifted of wavelength with fluid volume increased, λ = 324.6 nm, λ=327.9 nm, λ=327.9 nm for 8 ml, 16 ml, 25 ml respectively as shown in Figure.5.16, after annealing the absorption A increased from 0.357 to 0.531 for 8 ml. 0.53 for 16 ml becomes 0.66, while for 25 ml 0.532; Figure 5.17 a, b, and c explains these results. There is no obvious change in wavelength shifting in other words, the annealing has a slight impact on the bandgap value also fluid volume has slight effect to decrease the bandgap value. The most important thing about the doping is to control the dopant concentration because if its reach to a certain extent it will give an adverse result that means increase bandgap with a higher ratio of dopant that due to the formation of the secondary phase of Zn_2TiO_4 on Rutile TiO_2 surface (Wu et al., 2016). There is another reason which is the formation of restricting d-states within the TiO_2 band gap, that will lead to all the holes transport from the valence band VB and the electrons in the conduction band CB band will capture by restricting d-states so this will lead to increased band gap value (Kessler, 2014).

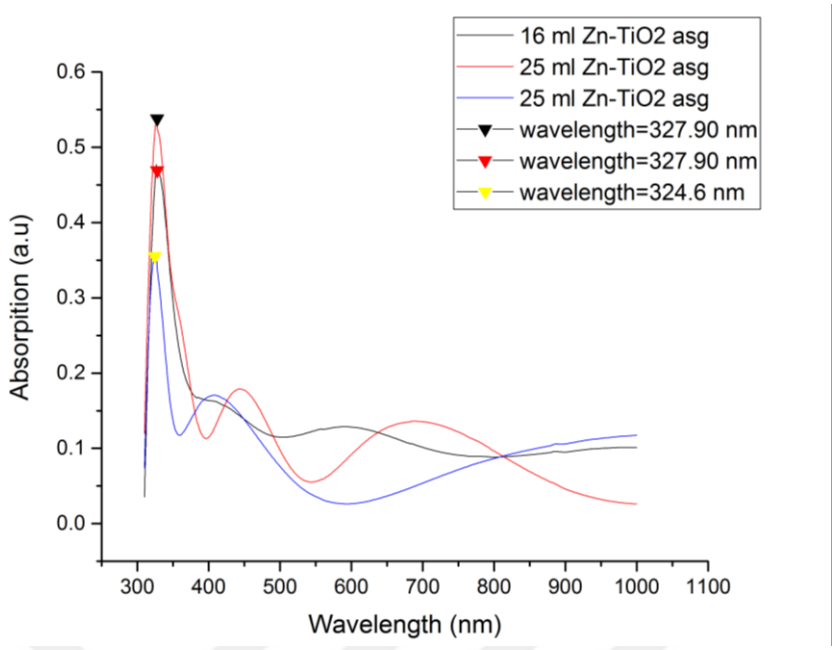

Figure 5.17. The relation between wavelength and absorption of a Zn-TiO_2 thin film for different fluid volume

a)

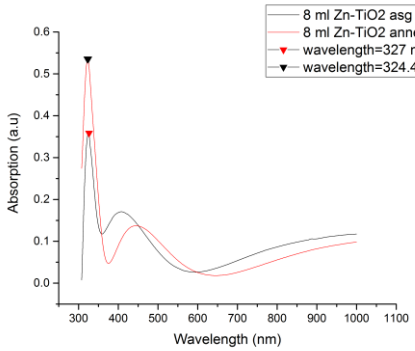

b)

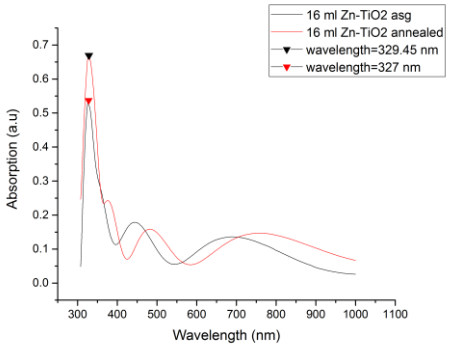

c)

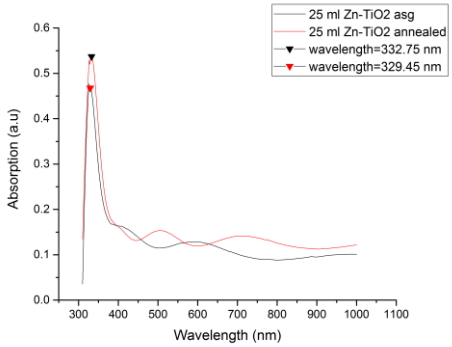

Figure 5.18. a, b, and c the relation between wavelength and absorption of a Zn-TiO_2 thin film for 8 ml,16 ml, 25 ml respectively

Table 5.11. The relation between wavelength λ and bandgap for as-grown samples

Fluid volume (ml)	λ (nm)	E_g (eV)
8	324.6	3.82
16	327.9	3.78
25	326.9	3.78

Table 5.12. The relation between wavelength λ and bandgap for annealed samples

Fluid volume (ml)	λ (nm)	E_g (eV)
8	324.41	3.84
16	329.45	3.76
25	332.75	3.72

From Tauc equation; $\alpha h\upsilon = A(h\upsilon - E_g)^n$, where α is the absorption coefficient which calculated by ($\alpha = 2.303\, A/t$) where t is the film thickness that obtain from SEM image (~ 420, 280 and 140 nm for 25, 16, 8 ml annealed samples sequentially), and A is the Absorption, hυ is the photon energy, and n is the depend on electronic transition type and it is equals to (1/2) for direct transition. So after plot the graph between $(\alpha h\upsilon)^2$ and $h\upsilon$ we can obtain the bandgap value E_g=3.493, 3.473 and 3.498 eV for 8 ml,16 ml and 25 ml annealed samples respectively, as shown in Figure 5.19. The result from Tauc equation is compatible with the result that got it from wavelength equation ($E_g = hc/\lambda$) for the peak position of absorbance spectra.

a)

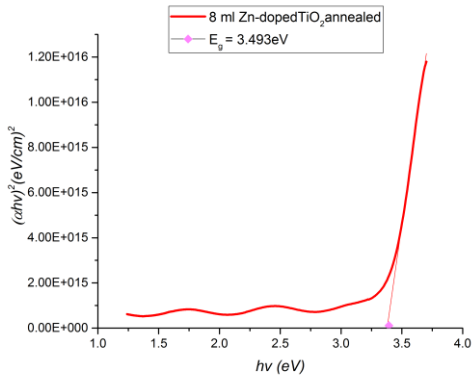

b)

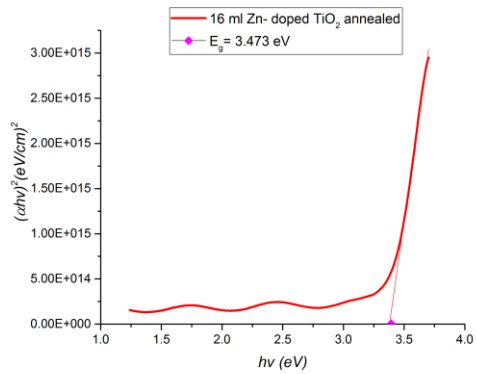

c)

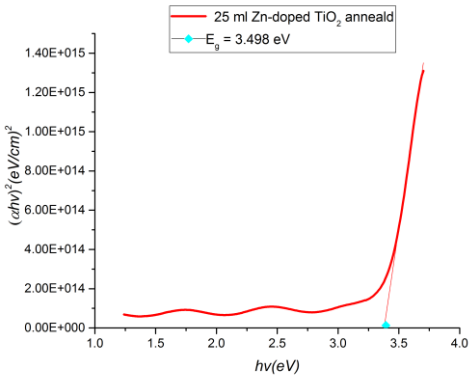

Figure 5.19. The bandgap value from Tauc equation for a) 8 ml, b) 16 ml, c) 25 ml annealed samples

5.5. The Electrical Characterization of Dye-Sensitized Solar Cell

The electrical properties for the dye-sensitized solar cell was investigated by Current-Voltage measurement system (Keithley 2400 sourcemeter and Solar Light Sun Simulator with AM 1.5 Filter) according to result the device behaved look like solar cell, but the efficiencies were low (~ 1.12 %) for bare TiO_2 (~ 1.04 %) for Zn doped TiO_2 to explain that results; first low efficiency back to many reasons; such as the composition of solvent, solution concentration, quality of the dye, counter carbon electrode, series resistance of the cell structure and precision of production. In other hand decreasing in efficiency after doping cause it by increased bandgap because of high concentration of Zinc doping which is explained in (2.3.3. paragraph) that have a direct impact on electrical Fill Factor (FF), so after looking to Figure 5.19 and 5.20. it is clear FF for bare TiO_2 (FF = 32.9) is bigger than FF for Zn doped TiO_2 (FF = 24.5) that is opposite of the expected results, but there is a positive effect of doping on current density value which is increased after doping from 0.0086 A/cm^2 to 0.011 A/cm^2. That means the photogenerated electron number increased after Zn doping of TiO_2 thin films. After morphological study for our film which is indicate porous nature and dense of particle that causes increased electron mobility (grain size effects) , also high concentration of Zinc doped decreased resistivity that is because amended crystallinity, so produce DSSC device with doped film more benefit than non-doped film, provided that determination of doping ratio, that was reported in many research; the resistivity for bare TiO_2 ~ 3.42×10^2 Ω.cm while its became 2.03×10^2 Ω.cm for 8 at.% of Zn-doped TiO_2 (Arunachalam et al., 2015). But

inhomogeneous solar cell structures (counter electrode quality, iodide solution etc.) caused series resistance problems.

From the current-voltage measurements which can be seen in Figure 5.19 and 5.20, the efficiency of the solar cell (η) can be calculated by the following equation:

$$\eta = \left(\frac{V_m \times I_m}{P_{in}}\right) \times 100\% \quad (5.2)$$

where, the voltage at maximum point V_{mp}, the current at maximum I_{mp}, and the incoming power P_{in} which equal to solar energy (0.104 W/cm^2).

For the electrical FF of fabrication DSSC which is calculated by the equation:

$$FF = \left(\frac{V_m \times I_m}{V_{oc} \times I_{sc}}\right) \times 100\% \quad (5.3)$$

where, the open circuit voltage V_{oc}, while the short-circuit current I_{sc}. The results above are summarized in Table 5.13.

Table 5.13. Comparison between bare TiO_2 and doped TiO_2 for DSSC parameters

The values	**TiO_2**	**Zn doped TiO_2**
I_{SC} (A/cm^2)	0.0087	0.0114
V_{oc} (V)	0.410	0.401
I_m (A/cm^2)	0.0052	0.0057
V_m (V)	0.227	0.189
FF (%)	32.9	24.5
Efficiency (% η)	1.12	1.04

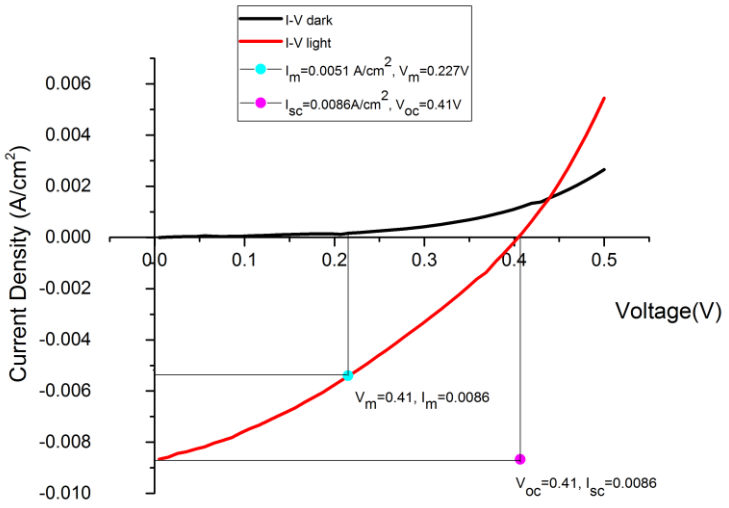

Figure 5.20. Current-Voltage curve for DSSC of bare TiO_2 dark - light

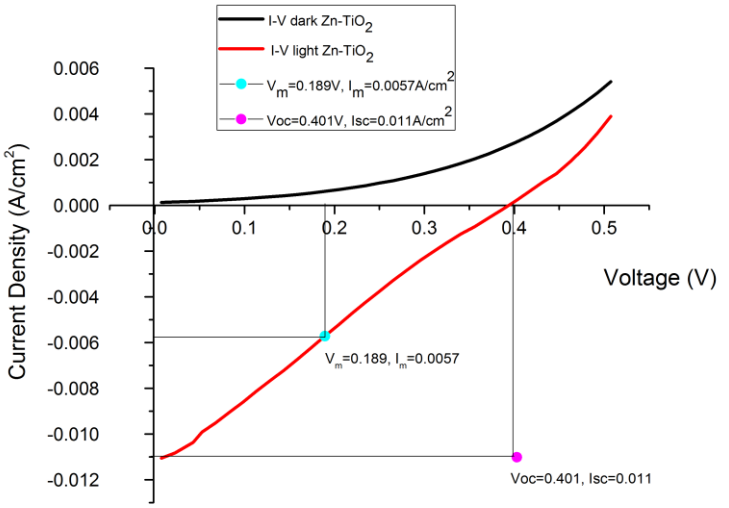

Figure 5.21. Current-Voltage curve for DSSC of Zn doped TiO_2 dark - light

6. CONCLUSION

Zn-doped TiO_2 (Zn:TiO_2) thin film deposited by Ultrasonic Spray Pyrolysis (USP) deposition technique on a glass substrate. The films are annealed up to 550 ˚C under atmosphere. After that, the surface morphology was studied by SEM measurement, to calculate the roughness of the thin film surface investigated by AFM Measurements, and the structural properties of the film measured by XRD system. To calculate the band gap of Zn-doped TiO_2 optical properties has been verifying after all that studied it was be found that the nature of the film suitable to DSSC applications. For device application Zn-doped TiO_2 deposited on ITO glass substrate annealed up to 470 ˚C and then soaked in Ru ruthenium (II) dye. Another ITO glass substrate used as an anode after covering it with graphite. The two substrates stick together, then the iodide electrolyte that has been injected between the substrates. The electrical properties of the device were also studied.

For deposition part: USP technique has many features such as simple to use, cheaper than other deposition technique, no need for complicated preparation because its open access chamber, it can be used for wide area thin film formation, and etc. In other hands, controlling the experiment parameters determines our film characteristic like crystal orientation, phase, particles size, the thickness of film, morphology, and distribution of particles. For example; the distance between the nozzle and substrate has a direct effect on the distribution of the atomizing particles and so on, crystal phase. That distance fixed according to nozzle type; in our work the distance was 9 cm and that value effect on our film and make it that form or; increase substrate temperature above 250 ˚C created dry layer without cracks or damp layer, in other words: XRD showed the crystal size of the thin films increased from 116 Å to 505 Å by increasing the annealing temperature which happened due to the grain boundary improvement. That makes grain size increase due to the harmony between the neighboring grains after removing their common boundaries, which is caused by enough temperature of annealing. The Anatase TiO_2 peak appears after annealing the samples up to 400 ˚C, in other hands we compared the result for different fluid volume the comparison refers to that the increase of fluid volume increased thickness

of film without effect on crystal size even though for different annealing temperature. It can be seen that the mean structure of our films is tetragonal of Anatase (66.7%) TiO_2, there are also Rhombo.H.axes (9.6%) TiO_2, $Zn_2TiO_3O_8$ Zinc Titanium Oxide cubic phase (22.6%), and TiZn Titanium Zinc in cubic form (1.1%) phases. The appearance of extra crystal phases except pure Anatase TiO_2 are due to high Zn dopant atoms concentration, the way that takes their positions in the lattice by doping.

SEM images exhibit a porous nature of the film, which makes it suitable for fabrication of DSSC by increasing the active surface area. But increased the fluid volume up to 25 ml (more than 400 nm thickness) decreased the strain of the film which makes the cracks appeared also the annealing made the same effect, and increased the size of cracks due to the expansion in lattice parameter. But it helped to move the boundary which causes disappearance the bulk particles, thus more homogenous thin film.

For EDS analysis, there is no effect of annealing on elements weight or atomic percentage. Because of the open atmospheric chamber of our experiment, there is a high atomic percentage of O_2 (52 % - 87 %) and it also increases by annealing as expected. The high percentage error value for Zinc element is due to the ratio of doping.

The decreasing of roughness after annealing was obvious from AFM result that makes our film suitable to use as a compact layer in organic (Dye sensitized, Perovskite etc.) solar cell. The roughness of the film increased with fluid volume increasing and decreased with increasing of annealing temperatures.

According to UV-Vis measurement; the band gap value increased after Zn doping, because the high concentration of doping. For annealed samples there is no marked change in bandgap value also for different fluid volume deposition. The value of bandgap that calculated from Tauc equation familiar to that we have got it from the equation ($E_g = hc/\lambda$) and they are close to theoretical results. The previous studies

refer to decreased of bandgap value after metal doping but it is only permissible for specific ratios of doping concentration that means high concentration of doping material leads to formation of restricting d-states which is an internal level formed within bandgap, so holes transport from the valence band VB and the electrons in the conduction band CB band will capture by this level, in other words the, band gap depends on dopant concentration and there is no obvious effect of annealing on its value. In other word; the annealing improved crystallinity, dispose of bulk particle, decreased roughness of film, and increased homogeneity, but it has no marked effect on band gap value, absorption, shifting of wave length. By changing the parameters such as annealing temperatures, solution concentration, solvent type, temperature of deposition, it can be controlled the nature of the thin film as if it smooth and compact to use for perovskite solar cell or porous for DSSC applications.

After Zn:TiO_2 film characterization, a DSSC device produced then electrical properties under dark and light were studied. The results showed that, the device have low efficiency (η = 1.04 %), decreased in electrical Fill Factor (FF = 24.5), and increased in current density (I_{sc} = 0.011 A/cm^2) after Zn doping. There is an increment in photogenerated current. It is clear from UV measurement which is indicated increasing in bandgap value because of augmentation of electron capture, multiple phases of $ZnTiO_2$ after formed d-states within bandgap due to high concentration of Zinc doping. But there is a low power output because of the high serial resistivity of device structure and electron-hole recombination inside the iodide solutions.

In the viewpoint of this study, possible future works by using USP technique there are a few critical parameters which must be well arranged such as: composition of solvent (solvent kind, dopant, and their concentration), solution flow rate, substrate temperature, distance between substrate and nozzle, and the most important factors is definition of Zinc doping ratio which is according to our experimental results must be less than 8 at. %. For solar cell device production by using USP technique with many types of dye to produce multiple solar cells will be our future works.

REFERENCES

Arunachalam, A., S. Dhanapandian, C. Manoharan, and G. Sivakumar. 2015. "Spectrochimica Acta Part A : Molecular and Biomolecular Spectroscopy Physical Properties of Zn Doped TiO_2 Thin Films with Spray Pyrolysis Technique and Its Effects in Antibacterial Activity." Spectrochimica Acta Part A: Molecular And Biomolecular Spectroscopy (2015) 138 105-112 DOI: 10.1016/j.saa.2014.11.016

Asahi, R. 2012. "Visible-Light Photocatalysis in Nitrogen-Doped Titanium Oxides." 269(2001) Journal of Asynchronous Learning Network (2012) 16(5) 61-71 DOI: 10.1126/science.1061051

Blade, Doctor, A. Berni, M. Mennig, and H. Schmidt. 1952. "2.2.8 Doctor Blade." 8–11 Boston, MA, Springer US, (2004), 89-92 DOI: 10.1007/978-0-387-88953-5_10

Chowdary, Mohana Krishna, Vijay Sekhar Babu, Govinda Rao, and Surya Prakash. 2012. "Synthesis of Nano Titanium Dioxide Powder Using MWP (Microwave Plasma) and Its Characterization." 2(3):1150–56 ISSN: 1792-4308 Advanced Research In Physics And Engineering *(2010).*

Chu, Yinghao. 2011. "Review and Comparison of Different Solar Energy Technologies August 2011 Table of Contents." (August) echnologies RGENI (2012) (14) 2756-2765 DOI: 10.1002/ejoc.201200111.

Cotutelle, E. N., Avec L. Universite, L. Université D. E. Trento, and M. Lorenzo Pavesi. 2013. "Growth By Radio Frequency Sputtering And Characterisation Of Rare Earth Doped Wide Bandgap OxideS Thesis for Doctra."

Essalhi, Z., B. Hartiti, A. Lfakir, M. Siadat, and P. Thevenin. 2016. "Optical Properties of TiO_2 Thin Films Prepared by Sol Gel Method." 7(4):1328–3 J. Mater. Environ. Sci. 7 (4) (2016) 1328-1333 Essalhi et al. ISSN : 2028-2508 CODEN: JMESCN 3.

Förster, H. 2004. "UV / VIS Spectroscopy." *Mol. Sieves* 4:337–426 www.asahi.com/ajw/articles/AJ201710020039.html DOI: 10.1007/b94239.

Hamedani, Hoda Amani. 2008. "Investigation of Deposition Parameters in Ultrasonic Spray Pyrolysis for Fabrication of Solid Oxide Fuel Cell Cathode Copyright 2008 By Hoda Amani Hamedani Investigation of Deposition Parameters in Ultrasonic Spray Pyrolysis for Fabrication Of." *Materials Science* (December).

Harjee, Nahid. 2013. "Energy Proportional Memory Systems a Dissertation Submitted To the Department of Department of Electrical Engineering and the Committee on Graduate Studies of Stanford University in Partial Fulfillment of the Requirements for the Degree Of." (August) Phd thesis.

Kessler, Fondazione Bruno. 2014. “A Review of TiO_2 Nanoparticles.”Chinese Science Bulletin (2011) 56(16) 1639-1657 DOI: 10.1007/s11434-011-4476-1

Khairy, M. and W. Zakaria. 2014. “Effect of Metal-Doping of TiO 2 Nanoparticles on Their Photocatalytic Activities toward Removal of Organic Dyes.” Egyptian Journal Of Petroleum.

Kojima, Akihiro, Kenjiro Teshima, Yasuo Shirai, and Tsutomu Miyasaka. 2009. “Organometal Halide Perovskites as Visible-Light Sensitizers for Photovoltaic.” 6050–51 Journal of the American Chemical Society (2009) 131(17) 6050-6051 DOI: 10.1021/ja809598r.

Kumar, Subodh. 2006. “Spectroscopy of Organic Compounds.” Dept. of Chemistry 66:1–36 Dept. of Chemistry,Guru Nanak Dev University DOI: 10.3945/jn.114.208066.

Li, Quan-jun and Bing-bing Liu. 2016. “High-Pressure Structural Phase Transitions of TiO_2 Nanomaterials .” 25(7):1–9 Chinese Physics B DOI: 10.1088/1674-1056/25/7/076107.

M. Umar and H. Abdul Aziz. 2013. “World ’ s Largest Science, Technology & Medicine Open Access Book Publisher Photocatalytic Degradation of Organic Pollutants in Water.” ntech (2012) 6 111-133 DOI: 10.5772/711.

Manser, Joseph S., A. Christians, and Prashant V Kamat. 2016. “Intriguing Optoelectronic Properties of Metal Halide Perovskites.” American Chemical Society. https://doi.org/10.1021/acs.chemrev.6b00136.

Muscat, Joseph, Varghese Swamy, and Nicholas M. Harrison. 2002. “First-Principles Calculations of the Phase Stability of TiO_2” 65:1–15 Physical Review B - Condensed Matter and Materials Physics, 65(22), 2241121–22411215. https://doi.org/10.1103/PhysRevB.65.224112.

Ni, Meng, Michael K. H. Leung Ã, Dennis Y. C. Leung, and K. Sumathy. 2007. “A Review and Recent Developments in Photocatalytic Water-Splitting Using TiO_2 for Hydrogen Production.” 11:401–25 Renewable and Sustainable Energy Reviews. DOI:10.1016/j.rser.2005.01.009.

Nowotny, M. K., L. R. Sheppard, T. Bak, and J. Nowotny. 2008. “Defect Chemistry of Titanium Dioxide . Application of Defect Engineering In.” Journal of Phys Chem, 112, 5275–5300. https://doi.org/10.1021/jp077275m.

Pahade, Vishakha S., Pankaj S. Chavan, and Vaishali P. Baisane. 2016. “A Review Paper on Vapour Deposition Coating.” (6):75–78 International Journal of Engineering and Applied Sciences (IJEAS).

Pingali, Kalyana C., David A. Rockstraw, and Shuguang Deng. 2005. “Silver

Nanoparticles from Ultrasonic Spray Pyrolysis of Aqueous Silver Nitrate." Aerosol Science and Technology, 39(10), 1010–1014. https://doi.org/10.1080/02786820500380025.

Richner, Roy P. 2001. "Research Collection Doctoral Thesis Thin Film Deposition by Spray Pyrolysis and the Application in Solid Oxide Fuel Cells." 12–19 Sang Thrombose Vaisseaux DOI: 10.3929/ethz-a-010782581.

Ruzybayev, Inci, Emre Yassitepe, Awais Ali, and A. S. Bhatti. 2015. "Materials Science in Semiconductor Processing Reactive Pulsed Laser Deposited N – C Codoped TiO_2 Thin Films." 39:371–76 DOI: 10.1016/j.mssp.2015.05.013.

Savale, P. a. 2016. "Physical Vapor Deposition (PVD) Methods for Synthesis of Thin Films: A Comparative Study." Archives of Applied Science Research 8(5):1–8.

Seshan, Krishna. 2001. Handbook Of Thin-Film Deposition Processes And. 2nd edition. published in the United States of America by Noyes Publications.

Tanaka, Keiichi, Mario F. V Capule, and Teruaki Hisanaga. 1991. "Effect of Crystallinity of $Ti0_2$ on Its Photocatalytic Action." 187(1):2–5 Chemical Physics Letters (1991) 187(1-2) 73-76 DOI: 10.1016/0009-2614(91)90486-S.

Tyona, M. D. 2013. "A Theoretical Study on Spin Coating Technique." Adv. Mater. Res. 2(4):195–208 Advances in materials Research (2013) 2(4) 195-208 DOI: 10.12989/amr.2013.2.4.195.

Unruersrty, Hokkaido 1986."Photocatalytic Activity Of No,-Doped In The Visible Light Region" Shinri. 123(1):126–28 ISSN: 0730-7268.

Wu, Ming-Chung, Shun-Hsiang Chan, Meng-Huan Jao, and Wei-fang Su. 2016. "Solar Energy Materials & Solar Cells Enhanced Short-Circuit Current Density of Perovskite Solar Cells Using Zn-Doped TiO 2 as Electron Transport Layer." Solar Energy Materials and Solar Cells 157:447–53.

Xie, Meng-yu, Kang-yang Su, Xin-yuan Peng, Ren-Jang Wu, and Murthy Chavali. 2017. "Journal of the Taiwan Institute of Chemical Engineers Hydrogen Production by Photocatalytic Water-Splitting on Pt-Doped TiO_2 – ZnO under Visible Light." Journal of the Taiwan Institute of Chemical Engineers 70:161–67.

Yuri F. Zhukovskii, Sergey Piskunov, Oleg Lisovski, Andrei Chesnokov and Dmitry Bocharov. 2016. "World ' s Largest Science, Technology & Medicine Open Access Book Publisher First Principle Evaluation of Photocatalytic Suitability".

Z.Yahya, Khaled. 2010. "Characterization of Pure and Dopant TiO_2 Thin Films for Gas Sensors Applications." (June) Phd thesis.

Zaleska-medynska, Adriana and Adriana Zaleska. 2017. “Doped-TiO_2 : A Review Doped-TiO_2 : A Review.” (November 2008) Recent Patents on Engineering (2008) 2(3) 157-164 DOI: 10.2174/187221208786306289.

Zallen, R. and M. P. Moret. 2006. “The Optical Absorption Edge of Brookite TiO 2.” 137:154–57 olid State Communications (2006) 137(3) 154-157 DOI: 10.1016/j.ssc.2005.10.024

Zehe, A. 2001. “Thermal Response of a Knudsen-Type Effusion Source to Sudden Heating-Power Changes ” 72–76 Superficies y Vacío, 13, 72–76.

Internet Cite Reference

Alechetron, 2018 "Perovskite (structure)" Access time: 13.8.2018. https://alchetron.com/Perovskite-(structure).

Babak Olyaeefar SohrabAhma di-Kandjani AsgharAsgari 2017 "Bulk and Interface Recombination in Planar Lead Halide Perovskite Solar Cells: a Drift-Diffusion Study" Access time: 13.8.2018. https://doi.org/10.1016/j.physe.2017.07.018.

Best Research-Cell Efficiencies" Chart – NREL Access time: 13.8.2018. https://www.nrel.gov/pv/assets/pdfs/pv-efficiencies-07-17-2018.pdf.

BlackHoleLab 2018 "Spin Coating PDMS Membrane" _ Application Note" Access time: 13.8.2018. http://www.blackholelab-soft-lithography.com/blackholelab-soft-lithography-stations-faq/how-to-do-a-spin-coated-pdms-membrane.

Chamandy.org 2014 "What is titanium dioxide doing in our food" Access time: 13.7.2018. https://chamandy.org/2014/11/23/what-is-titanium-dioxide-doing-in-our-food.

Chi-Hung Liao, Chao-Wei Huang, and Jeffrey C. S. Wu, Catalysts 2012 " Hydrogen Production from Semiconductor-based Photocatalysis via Water Splitting" Access time: 20.7.2018. http://www.mdpi.com/2073-4344/2/4/490.

Fatima Javed, Hina Zakir, and Maira Nazneen research at. 2015 "Synthesis and Characterization Of Titanium Dioxide Thin Films Using Spin Coating Technique" Access time: 13.7.2018. https://www.researchgate.net/Figure/a-Crystal-structure-b-Physical-form-of-Anatase_Figure4.

Gamry Instruments 2018 "DSSC: Dye-Sensitized Solar Cells Basic Principles and Measurements" Access time: 13.8.2018. https://www.gamry.com/application-notes/physechem/dssc-dye-sensitized-solar-cells.

Sigmaaldrich 2007 http://large.stanford.edu/courses/2007/ph210/hellstrom1. https://www.sigmaaldrich.com/materials-science/material-science-products.html?TablePage=108832720.

IndiaMart 2018 "Spin Coater" Access time: 13.8.2018. https://dir.indiamart.com/impcat/spin-coater.html.

Large Stanford 2007" Basic Models of Spin Coating" Access time: 13.8.2018.

Muhammad Umar and Hamidi Abdul Aziz, INTECH 2013 "Photocatalytic Degradation of Organic Pollutants in Water" Access time: 20.7.2018.

People Chem Ucsb Edu 2012" Description of the Electronically Excited States" Access time: 13.8.2018 https://people.chem.ucsb.edu/kahn/kalju/chem126/public/elspect_theory.html

Rajesh Pandiyan.2013 " Growth by Radio Frequency Sputtering and Characterisation Of Rare Earth Doped Wide Bandgap Oxides" Access time: 13.8.2018. http://eprintsphd.biblio.unitn.it/1057/1/Rajesh_Pandiyan_Thesis_Complete.

Sajid Ali Ansari, Mohammad Mansoob Khan, Mohd Omaish Ansari 2016 "Nitrogen-doped titanium dioxide (N-doped TiO_2) for visible light photocatalysis" Access time: 13.8.2018. doi: 10.1039/C5NJ03478G.

Schanze Research Group 2014 "Dye-Sensitized Solar Cells" Access time: 13.8.2018. https://schanze.chem.ufl.edu/research/dye-sensitized-solar-cells.

Science Direct 2014" Dip coating of poly (ε-caprolactone)/hydroxyapatite composite coating on Ti6Al4V for enhanced corrosion protection" Access time: 13.8.2018. https://www.sciencedirect.com/science/article/pii/S08ml7897214001674.

Sigma Aldrich 2018 "Physical Vapor Deposition (PVD)" Access time: 13.8.2018.

Sono Tek 2016 "Ultrasonic Nozzle Spray Technology for Thin Film Coating" Access time: 13.8.2018 http://www.boelnordic.com/wp content/uploads/2016/03/sonotek_coating.pdf.

Teaching Advanced Physics 2018"Episode 530: X-ray diffraction" Access time: 13.8.2018 http://tap.iop.org/atoms/xray/530/page_47297.html.

Tmaxcn 1995 "Automatic Electrode Coater With 8"W X 13"L Vacuum Chuck & 180mm Doctor Blade" Access time: 13.8.2018. https://www.tmaxcn.com/automatic-electrode-coater-with-8-w-x-13-l-vacuum-chuck-180mm-doctor-blade_p493.html.

CURRICULUM VITAE

Personal Information:

Name	: ZINAH HAFEDH AL-SALIHI
Place and Date of Birth	: Iraq - 26/10/1978
Marital Status	: Married
Foreign Language	: English, Arabic
Nationality	: Iraqi
Email	: zozotaha1978@gmail.com

Education:

High school	: Baghdad high school, 1997.
Undergraduate Education	: Baghdad University/College of Education/Department of Physics 2001.

Publications

This work has been published as an oral presentation in "*ICSMD 2017 international congress on semiconductor materials and devices*".

ÖZGEÇMİŞ

Kişisel Bilgiler:

Adı ve Soyadı	: ZINAH HAFEDH AL-SALIHI
Doğum Yeri ve Yılı	: Diali-Irak
Medeni Hali	: Evli
Yabancı Dili	: İngilizce, Arapça
Uyruğu	: Irak
E-posta	: zozotaha1978@gmail.com

Eğitim Durumu:

Lise	: Bağdat Lisesi, 1997.
Lisans Öğrenimi	: Bağdat Üniversitesi / Eğitim Fakültesi /Fizik bölümü.

Yayınlar

Bu çalışma "*ICSMD 2017 Uluslararası Yarı İletken Malzemeler ve Cihazlar Kongresi*" nde sözlü olarak sunulmuştur.